J. Fluid Mech. (2015), *vol.* 768, *pp.* 261–293.
doi:10.1017/jfm.2014.743

The wall-pressure spectrum of high-Reynolds-number turbulent boundary-layer flows over rough surfaces

Timothy Meyers[1], **Jonathan B. Forest**[1] **and William J. Devenport**[1,†]

[1]Department of Aerospace and Ocean Engineering, Virginia Polytechnic Institute and State University, Blacksburg, VA 24061, USA

(Received 28 January 2014; revised 16 December 2014; accepted 19 December 2014; first published online 9 March 2015)

Experiments have been performed on a series of high-Reynolds-number flat-plate turbulent boundary layers formed over rough and smooth walls. The boundary layers were fully rough, yet the elements remained a very small fraction ($<1.4\,\%$) of the boundary-layer thickness, ensuring conditions free of transitional effects. The wall-pressure spectrum and its scaling were studied in detail. One of the major findings is that the rough-wall turbulent pressure spectrum at vehicle relevant conditions is comprised of three scaling regions. These include a newly discovered high-frequency region where the pressure spectrum has a viscous scaling controlled by the friction velocity, adjusted to exclude the pressure drag on the roughness elements.

Key words: boundary layer structure, turbulent boundary layers

1. Introduction

The practical and environmental conditions of almost all large-scale fluid dynamic applications ensure that the flow surfaces are rough. The roughness intensifies and changes the scaling and character of the fluctuating pressure field experienced on those surfaces. These boundary-layer pressure fluctuations are of engineering interest since they are responsible for flow-induced noise and vibration. They are also of scientific interest because they provide a measure of the turbulence structure of the boundary layer weighted in favour of the near-wall dynamics. Despite their importance, remarkably little is known about pressure fluctuations produced by rough-wall boundary layers. The absence of data is particularly acute for practically-relevant conditions that combine high Reynolds numbers and large boundary-layer thickness to roughness size ratios, conditions at which universal scalings and behaviours are most likely to be observed. The broader purpose of the research reported here is to fill this knowledge gap through experimental measurements. In this paper, we focus on the wall-pressure spectrum and its frequency scaling.

The fundamental fluid dynamics of rough-wall boundary layers (without reference to wall pressure) has been reviewed by Jiménez (2004). Almost all practical rough walls are 'k-type', typified by the classic sand-grain roughness experiments of Nikuradse

†Email address for correspondence: devenport@vt.edu

(1950). The effect of such roughness on the mean velocity profile is to shift the logarithmic region. Following Nikuradse, the shift can be characterized in terms of a comparative distance k_s referred to as the equivalent sand-grain roughness. It is important to note that k_s is dependent on the aerodynamic effects of a rough surface, and thus part of the flow solution, rather than a parameter that can be inferred *a priori* from a particular rough surface shape. The equivalent sand-grain roughness is usually greater than the geometric height of the roughness k_g, but dimensional analysis suggests that for larger roughness sizes the two should be proportional. In practice k_s/k_g is expected to become constant around a roughness Reynolds number $k_g^+ = k_g U_\tau/\nu \approx 80$, where U_τ is the friction velocity and ν is the kinematic viscosity. Above this threshold (where the roughness elements project into the log layer) the surface is conventionally termed 'fully rough'. This is the regime of broadest practical application and the one where scaling laws will be most apparent. In this regime, the skin friction is usually thought of as due to form drag on the roughness elements (Simpson 1973). Below this threshold (where the roughness elements are serving to disrupt the mechanics of the buffer layer), roughness effects become influenced by geometry-dependent viscous drag mechanisms, and the term 'transitional roughness' is used.

The vertical scale of the roughness k_g is also important in relation to the boundary-layer thickness δ. Jiménez (2004) notes that, for boundary layer to roughness size ratios δ/k_g less than approximately 50, the roughness disrupts the bulk of the log layer and such flows may be better understood as flows over obstacles, which are again dependent on the roughness geometry details. While the value of 50 should only be thought of as a rough guideline, it is clear that in most practical applications δ/k_g will be substantially greater than this value and thus presumably large enough for the details of the roughness geometry to be unimportant. It is in this regime that the most scientifically interesting and practically useful scaling behaviour should be observed. It is expected that at high δ/k_g the turbulent boundary layer should display wall similarity (Raupach, Antonia & Rajagopalan 1991) so that the outer portions of the boundary layer become independent of the details of the roughness. Flack, Schultz & Shapiro (2005) and Schultz & Flack (2007) present measurements of transitionally and fully rough turbulent boundary layers with large δ/k_g that appear closely consistent with this expectation.

The dual requirement of high k_g^+ and high δ/k_g implies a boundary-layer-thickness Reynolds number $\delta^+ = \delta U_\tau/\nu$ of at least 4000. Few existing data sets meet these criteria, and almost none are concerned with the behaviour of pressure fluctuations at the wall. The absence of studies at high-Reynolds-number, high-scale-ratio conditions is an understandable consequence of the fact that most research of this type is conducted in laboratory-scale wind tunnels. The speed and size limitations of most of these facilities practically guarantees that large roughness Reynolds numbers cannot be achieved except with roughness elements that are large compared to the boundary-layer thickness.

The roughness height is, of course, only one measure of the geometry of a rough surface. The sparseness of the roughness elements λ, defined as the forward projected area of the elements divided by the wall area they cover, is another (Dvorak 1969). This parameter, which is discussed further by Simpson (1973) and George & Simpson (2000) among others, can be thought of as a measure of number density of roughness elements. When λ is small, the surface is characterized by a few widely separated roughness elements and the drag is low. As the number of elements and λ increase the drag increases, reaching a maximum at the point where adjacent elements begin

sheltering each other. At higher values of λ the sheltering effect is increased and the drag is reduced. Peak drag occurs at approximately $\lambda = 1/7$. Both k_g and λ are parameters that presume a surface composed of discrete elements or grains, and even then may represent an incomplete characterization of a rough surface. Precise characterization of the surface shape would seem to be an essential part of defining the boundary conditions of a repeatable rough-wall boundary-layer experiment.

The fully rough boundary layer is thought of as being achieved when the drag on the roughness elements has become essentially independent of viscosity and where the elements project into the log layer. While the condition cited above ($k_g^+ \gtrsim 80$) represents the traditional criterion for this behaviour, a significantly different view has been proposed by Mehdi, Klewicki & White (2010, 2013). Their arguments are based on insight from studies of smooth-wall boundary layers, most recently represented by the work of Klewicki, Fife & Wei (2009), Marusic *et al.* (2013), Meneveau & Marusic (2013) and Klewicki (2013), which indicate a four-layer structure to the boundary layer controlled by the relative importance of viscous forces, mean flow inertia and turbulent inertia (the latter represented by the Reynolds shear stress). One consequence of this is that significant viscous influence is thought to extend a much greater distance from the wall than previously envisaged, to a distance $y^+ \cong 3\sqrt{\delta^+}$. The four-layer structure introduces an additional distance scale given by the geometric mean of the viscous and boundary-layer scales $\sqrt{\nu\delta/U_\tau}$, a distance from the wall identified by Bradshaw (1967) as proportional to the centroid location of the Poisson equation integrand responsible for the wall-pressure fluctuations. For rough walls, Mehdi *et al.* (2010, 2013) argue that there is a region, extending above the tops of the roughness elements to the point y_m where the Reynolds shear stresses reach a maximum, where viscous forces will play a substantial role. This implies, at the very least, that the inertially dominated rough-wall flows assumed to characterize the fully rough condition may not appear until much higher roughness Reynolds numbers, if at all. Mehdi *et al.* (2010) introduce the averaged scales $\sqrt{k_s\delta}$ and $\sqrt{k_s\nu/U_\tau}$ as candidates for scaling the position of y_m and thus the position where the flow transitions to inertially dominated dynamics.

Pressure fluctuations at the wall of a turbulent boundary layer can be mathematically expressed through Poisson's equation as a weighted integral of source terms across the boundary layer (e.g. Chase 1980; Blake 1986). The weighting factor is of the form $\exp(-ky)$, where k is the wavenumber of the turbulence and y the distance from the wall. The implication is that the wall-pressure autospectrum will be dominated by contributions at high frequencies from turbulent structures close to the wall, and at low frequencies from larger-scale outer boundary-layer motions. As a result one expects low-frequency and high-frequency pressure fluctuations to obey different scaling laws.

This behaviour is fairly well established for smooth-wall boundary layers, for which there are numerous studies (see reviews by Willmarth 1975, Bull 1996 and Goody 2004, for example). Smooth-wall measurements in the very low-frequency range ($\omega\delta/U_\tau < 2$, see Panton *et al.* 1980; Farabee & Casarella 1991) show the autospectrum increasing as the square of the frequency, or slower. In the mid-frequency range, the pressure spectrum reaches a broad maximum and then begins to decrease, the maximum usually occurring near $\omega\delta/U_\tau \cong 2$ (though this value may be quite Reynolds number dependent, see Klewicki, Priyadarshana & Metzger 2008). Spectra in the low- to mid-frequency range are generally believed to scale on 'outer region variables' though there are differences of opinion on whether the appropriate scaling velocity is U_e (the edge velocity) or U_τ, and the appropriate distance is the boundary-layer displacement thickness δ^* or δ. Most authors (e.g. Bull 1996; Goody 2004) favour

normalizing the pressure spectrum level on the wall shear stress τ_w $(= \rho U_\tau^2)$. It is generally accepted that spectra in the high-frequency range conform to the Kolmogorov-type scaling, in which the pressure spectrum $\phi(\omega)$ is expected to be a unique function of frequency ω when normalized as $\phi(\omega)U_\tau^2/\tau_w^2\nu$ versus $\omega\nu/U_\tau^2$. The existence of two scalings has traditionally been taken to imply a universal overlap region where both apply. As argued theoretically by Bradshaw (1967) and Panton & Linebarger (1974), the spectrum should vary as ω^{-1} in this region. This slope does not appear to be achieved in practice, with most measurements (e.g. Blake 1970; McGrath & Simpson 1987) showing an exponent of -0.7 to -0.8. At the very high Reynolds numbers of atmospheric boundary layers, Klewicki *et al.* (2008) have shown an exponent of -1 for a flow over a transitionally rough surface.

The presence of roughness increases the overall wall shear stress and thus generally intensifies the turbulence in the boundary layer and the turbulent pressure fluctuations it produces. The roughness elements also introduce new local sources of pressure fluctuations as they shed vortices and as they respond to the unsteady inflow associated with the oncoming boundary layer (Yang & Wang 2013). There have been a number of studies where wall-pressure fluctuations have been measured in the presence of some roughness, but few where systematic studies of roughness effects have been performed. Major studies are summarized in table 1, illustrating the range of boundary-layer momentum-thickness Reynolds numbers, the surfaces, the range of roughness Reynolds numbers k_g^+, the ratio of boundary-layer thickness to roughness size δ/k_g, and the range of boundary-layer thickness to viscous-scale ratios $\delta^+ = \delta U_\tau/\nu$ studied. It is immediately apparent that there have been almost no previous studies of pressure fluctuations for rough-wall boundary layers with large enough k_g^+ ($\gtrsim$80) and δ/k_g ($\gtrsim$50) for the flow to be nominally free of transitional effects. Not surprisingly, therefore, these studies do not present a conclusive picture of the scaling or behaviour of pressure fluctuations under rough-wall boundary layers.

Blake (1970) performed a fairly comprehensive study of pressure fluctuations for a set of three rough surfaces. He made wind-tunnel measurements using pairs of microphones with 0.8 mm pinholes in an approximately 50 mm thick boundary layer. Experiments were performed at two free-stream speeds with a smooth wall and for three different rough walls producing momentum thickness Reynolds numbers of $Re_\theta = 21\,000$–$30\,000$. The latter consisted of 3 mm diameter grit particles scattered with an average spacing of 3.5, and 1.4 mm diameter particles scattered with average spacings of 4.9 and 2.8 mm. These cases, referred to by Blake as D-L (dense-large), S-S (sparse-small) and D-S (dense-small), respectively, all produced fully rough flows ($k_g^+ = 170$–410) with scale ratios (δ/k_g) from 26 to 42. Blake attempted to establish the scaling of the pressure autospectrum measured over these different surfaces. He used the outer-region boundary-layer scaling $\phi(\omega)U_e/\tau_w^2\delta^*$ versus $\omega\delta^*/U_e$ to collapse the lower-frequency portions ($0.3 < \omega\delta^*/U_e < 2.5$) of the spectra, which was found to work particularly well in correlating the smooth-wall and small-roughness cases (S-S and D-S). Blake proposed that pressure fluctuations at higher frequencies should scale as $\phi(\omega)U_\tau/\tau_w^2 k_g$ versus $\omega k_g/U_\tau$, though the collapse of his own measurements on this scaling was not perfect. Specifically, the largest roughness cases were least well correlated with this scaling and there appeared to be an effect of roughness spacing on spectral level.

Aupperle & Lambert (1970) also studied pressure fluctuations for boundary layers over a smooth wall and over walls roughened with grade 36, 12 and 4 grit particles spread randomly with an average particle spacing of approximately 4.6 diameters. Measurements were carried out for boundary-layer thicknesses ranging

https://doi.org/10.1017/jfm.2014.743 Published online by Cambridge University Press

	Surface	U_e (m s^{-1})	δ (mm)	δ^* (mm)	Re_θ	k_g (mm)	k_s (mm)	λ	k_g^+	k_s^+	δ/k_g	δ^+	U_τ/U_e
	S-S	38	60	13.9	21 200	1.43	2.69	—	177	333	41.9	7 400	0.0515
	S-S	50	60	14.6	29 800	1.43	2.69	—	233	440	41.9	9 800	0.0515
Blake (1970)	D-L	38	61	15.1	21 700	2.34	4.88	—	311	648	26.3	8 200	0.0565
Sand grains	D-L	50	61	15.1	28 800	2.34	4.88	—	412	861	26.3	10 900	0.0565
	D-S	38	58	13.3	21 200	1.43	1.87	—	172	224	40.9	7 000	0.0502
	D-S	50	58	13.3	28 000	1.43	1.87	—	227	296	40.9	9 300	0.0502
Aupperle &	Grade 36	50	28	3.6	—	0.50	2.50	0.047	81	405	56	6 400	0.074
Lambert (1970)	Grade 12	50	33	4.5	—	1.70	6.10	0.047	318	1141	20	8 900	0.0864
Sand grains	Grade 4	50	38	5.1	—	3.80	11.9	0.047	858	2687	10	12 200	0.1024
	Fetch 1	27	63	13.5	14 700	1.00	1.42	0.098	69	100	63.4	3 200	0.0412
	Fetch 1	20	64	12.5	10 300	1.00	1.42	0.098	52	72	64	4 400	0.0420
	Fetch 2	27	44	8.6	9 100	1.00	1.22	0.052	73	87	44.4	2 300	0.0446
Varano (2010)	Fetch 2	20	45	7.9	6 100	1.00	1.22	0.052	52	62	44.5	3 100	0.0439
Hemispheres	Fetch 3	27	30	5.1	5 700	1.00	0.43	0.025	74	33	30.4	2 500	0.0444
	Fetch 3	20	48	7.3	6 300	1.00	0.43	0.025	52	22	48.6	2 300	0.0426
	Fetch 4	27	60	8.5	10 200	1.00	0.39	0.013	65	26	59.7	2 700	0.0393
	Fetch 4	20	53	7.4	6 500	1.00	0.39	0.013	50	20	53.2	4 000	0.0402

TABLE 1. Summary of major rough-wall pressure studies.

from 28 to 38 mm depending on roughness, using ceramic transducers and pinhole microphones with 0.7 mm and 0.5 mm sensing diameters respectively. As shown in table 1, the grade 12 and 4 rough surfaces were fully rough, but had boundary-layer thickness to roughness size ratios well below that needed for the flow to be free of transitional effects. The 36 grit case, however, just meets Jimenez's criteria. Aupperle & Lambert paid particular attention to the exact placement of the roughness elements around the transducers, but found that it had almost no effect on the measured autospectrum, a finding confirmed in the study of Smith (2008). Their pressure spectra show levels that increase with roughness size at low frequencies (<7 kHz). Unlike Blake (1970) they show no outer boundary-layer scaling of their data. (Indeed, their measurements do not display the low-frequency maximum in the pressure spectrum seen in other data sets.) They do, however, find that the spectra for their three rough surfaces collapse when normalized on the inner roughness scaling $\phi(\omega)U_\tau/\tau_w^2 k_s C_f$ versus $\omega k_s/U_\tau$. Curiously, the collapse is worst at the highest frequencies $\omega k_g/U_\tau > 50$, where the inner scaling would be expected to be most appropriate. This is identical to Blake's (1970) inner scaling with the exceptions that the equivalent sand-grain roughness k_s is used in place of the geometric roughness size k_g and of the division of spectral level by the skin friction coefficient C_f. Blake (1971) argues that although this normalization collapses the spectra, it is more empirically based.

Varano (2010) examined the pressure spectra produced by a 43 mm thick boundary layer growing in air over a wall populated with 1 mm radius hemispheres in square arrays of 4, 5.5, 8, and 11 mm (termed fetches 1 to 4) at 20 and 27 m s^{-1}. Unlike Aupperle & Lambert (1970), Varano found that the pressure spectrum at high frequencies was quite strongly dependent on transducer placement relative to the roughness elements, and therefore compared different roughness cases looking only at pressure fluctuation measurements made at each roughness-cell centre, as far as possible from adjacent elements. Varano (2010) attempted to scale the high-frequency portion of the pressure spectrum first with Blake's (1970) and Aupperle & Lambert's (1970) scaling, finding that the former provided a fair collapse whereas the latter did not. He went on to argue that in the fully rough regime the friction velocity U_τ, should be proportional to the edge velocity U_e in which case Blake's scaling would become $\phi(\omega)/\rho^2 U_e^3 k_g$ versus $\omega k_g/U_e$. This scaling was found to produce comparable collapse to that of Blake (1970). Varano (2010) also concluded that element spacing was not an important factor when concerned with scaling the high-frequency surface-pressure spectrum.

There have been a few other scattered measurements of pressure fluctuations under rough-wall boundary layers. Willmarth & Wooldridge (1962) noted that pressure fluctuations measured with their smooth-wall configuration were increased by 25–50 % when the surface was left unfinished and when upstream fittings were left protruding slightly from the flow surface. Killen & Almo (1971) measured pressure fluctuations on a rotating roughened cylinder in a water tank, and clearly show an increase of pressure fluctuations with roughness size. Mulhearn (1976) studied the pressure fluctuations downstream of the start of a series of rectangular spanwise slots cut into the test wall. The slots were fully rough but quite large compared to the boundary-layer thickness ($\delta/k_g \cong 20$). Mulhearn saw significant differences in pressure spectra measured between the slots and in the slots. His data do not show rapid variations with distance downstream, but those variations which are visible appear to collapse with Blake's inner scaling. Klewicki *et al.* (2008) measured pressure fluctuations produced by the atmospheric boundary layer over the Utah desert, which they estimate to have been transitionally rough.

Evidence of the rough-wall pressure scaling from roughness noise measurements is also mixed. Farabee & Geib (1991) used a linear array of large-diameter microphones, placed downstream of roughness fetches, as a wavenumber filter. This enabled them to extract estimates of the intensity of the wavenumber frequency pressure spectrum at the acoustic wavenumber. They found the pressure fluctuations to scale in a manner consistent with Blake's (1970) outer scaling. Conversely, Hersh (1983) measured roughness noise emanating from the exhaust of a roughened pipe as a function of speed and roughness size and observed an approximate scaling that would be consistent with Blake's inner scaling with the geometric roughness size replaced by the effective sand-grain roughness.

In summary, we find that there have been no previous systematic studies of pressure fluctuations in rough-wall boundary layers with large enough roughness Reynolds number $k_g^+ \gtrsim 80$ and boundary layer to roughness scale ratio $\delta/k_g \gtrsim 50$ for the flow to be free of transitional effects. In other words, there have been no studies that have examined the rough-wall pressure fluctuations in the regime where universal scalings and behaviours are most likely to be observed, and where those scalings are of most practical and scientific value. The purpose of the present study is to therefore extend the existing database of boundary-layer fluctuating pressure measurements into this regime. In this paper we report on those measurements, focusing on the scaling of the wall-pressure time spectrum. We find that, for single-scale roughness elements, the boundary-layer pressure spectrum contains three distinct scaling regions, including a previously un-identified viscous scaling at the highest frequencies.

2. Apparatus and instrumentation

2.1. *Wind tunnel configuration*

This study was conducted in the Virginia Tech Stability Wind Tunnel. This facility is capable of generating flow speeds up to 80 m s^{-1} and has removable test sections 7.3 m long with square cross-sections of 1.83 m on edge. The anechoic test section (Devenport *et al.* 2013) employed for this study, has side walls made of a stretched Kevlar fabric that contain the flow while remaining acoustically transparent. Sound passing out of these is absorbed in one of two anechoic chambers flanking the test section. The floor and ceiling of the test section are also treated to minimize acoustic reflections. Turbulence levels in the closely uniform free stream of the empty test section are 0.024 % at 30 m s^{-1} and 0.031 % at 57 m s^{-1}.

To grow thick high-Reynolds-number turbulent boundary-layer flows within the anechoic test section, one of the Kevlar side walls was replaced with a hard surface consisting of six modular 1.22 m × 1.78 m framed Lexan panels (figure 1). The mounting arrangement allowed the position of each panel to be independently adjusted so as to form a continuous, smooth 1.78 m wide and 7.32 m long test surface with a near-zero pressure gradient.

The boundary-layer flow surface was located a nominal distance of 0.1 m inside the test section side wall to make room for the adjustment hardware. A 2.4 m × 2.4 m curved fairing with a smooth ABS plastic surface was used to create a gradual transition between the wind tunnel contraction and the leading edge of the surface (Morton 2012). Boundary-layer trips were mounted on the fairing at positions 1.2 m (primary trip) and 2.1 m (forward trip) upstream of the test surface leading edge. Both trips consisted of strips of 19 mm high aluminium angle mounted with the flange oriented downstream. This arrangement produced boundary-layer thicknesses in the test section downstream of over 0.2 m.

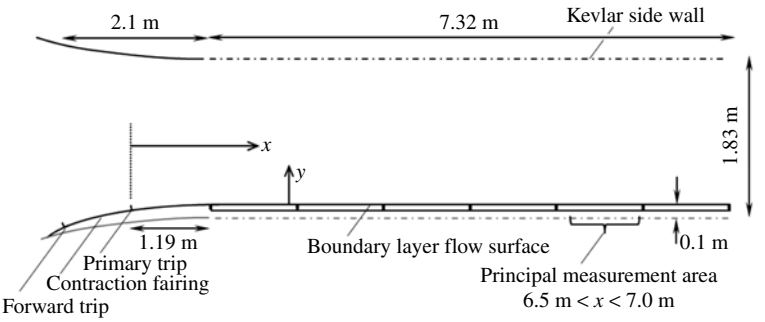

FIGURE 1. Test section configuration and coordinate system.

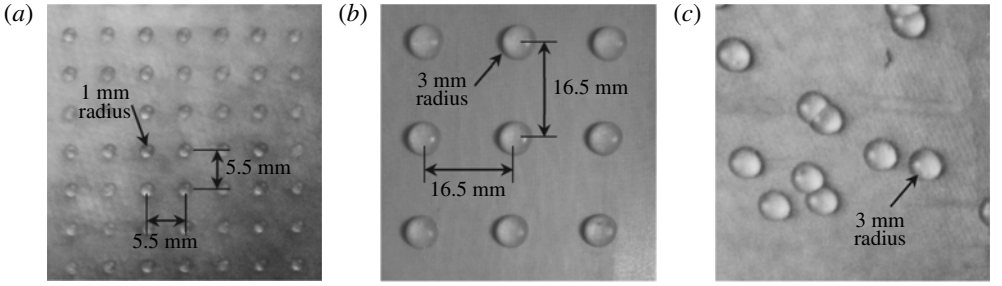

FIGURE 2. Rough surfaces (*a*) square array of 1 mm radius hemispheres, (*b*) square array of 3 mm radius hemispheres, (*c*) quasi-random distribution of 3 mm radius hemispheres.

2.2. *Rough surfaces*

Close-up photographs of the three rough surfaces tested are shown in figure 2. These consist of: a square array of 1 mm radius hemispheres with 5.5 mm spacing and with the rows of elements aligned with the flow direction; a scaled version of the first surface, with 3 mm hemispheres separated by 16.5 mm; a pseudo-random distribution of 3 mm surfaces with the same average element density as the second surface. (Data files containing a complete listing of the locations of all the elements in the pseudo-random surface can be obtained from the authors.) All three surfaces had the same sparseness ratio λ of 0.052, matching Varano's (2010) fetch 2. The surfaces were moulded from epoxy resin backed by paper and Kevlar, or paper and fibreglass, substrates. The 1.8 m wide and 1.2 m long moulded sections were then glued to 3 mm thick aluminium plates of the same size, designed to be bolted to the Lexan panels of the boundary-layer flow surface. The aluminium plates were shimmed to eliminate gaps or steps between adjacent sections of the rough surfaces. For the ordered surfaces, care was taken to ensure that the rows of roughness elements were aligned and contiguous between successive sections. The random surface was designed with a distribution of elements that was periodic over the 1.2 m length of each section so that there would be no interruption in the element pattern between adjacent sections. Note that the rough surfaces were only applied to the flat section of the test wall, so that each roughness fetch began 1.19 m downstream of the primary trip (figure 1). Figure 3 shows an overall view of the one of the roughness fetches (the 3 mm ordered array) installed. Both 3 mm hemispherical surfaces included close to 50 000 elements.

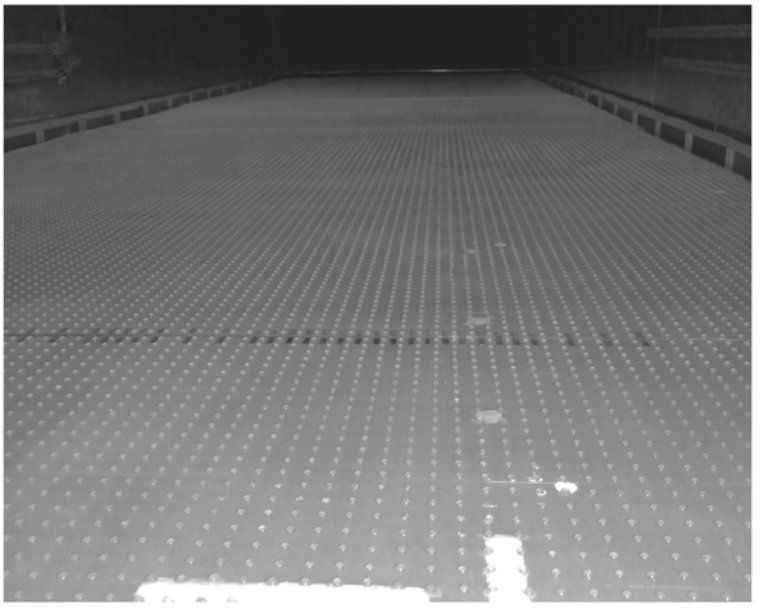

FIGURE 3. The 3 mm ordered array of hemispheres as installed and viewed from downstream. The width of the fetch is 1.8 m. The white components in the foreground are the surface-pressure microphone holders.

2.3. *Velocity instrumentation*

Velocity fluctuation measurements were made in the smooth- and rough-wall boundary flows using single- and four-sensor hot-wire anemometer probes. The four-sensor probes used (Auspex Corportation model AVOP-4-100) consist of two orthogonal arrays of X-wires within a 0.75 mm^3 measurement volume. This probe provides instantaneous measurement of the three components of flow velocity, with the redundant sensor reducing sensitivity to some gradient errors. Wittmer, Devenport & Zsoldos (1998) showed this type of probe to be capable of accurate Reynolds stress measurements to within 3 mm of a wall under conditions similar to those of the present study. Angle calibrations of the four-sensor probes were performed using the look-up table method of Wittmer *et al.* (1998). Single hot-wire probes used to provide near-wall measurements (Auspex Corporation model AHWU-100) consisted of a 1 mm-long sensor held perpendicular to the flow and parallel to the wall on a conventional arrangement of two parallel prongs.

Both single- and four-sensor probes were supported in the tunnel on a three-axis traverse gear with 0.025 mm resolution. Probes were supported from downstream on a 1 m long sting support so as to minimize any interference from the traverse. Sensors were operated in constant-temperature mode using constant-temperature anemometer bridges (Dantec Dynamics StreamLine) optimized to give a flat frequency response below 18 kHz. Anemometer signals were recorded using a 64-channel 16-bit Agilent E1432 digitizer. Probes were regularly calibrated for velocity in the wind tunnel free stream and corrected for temperature drift using the method of Bearman (1971).

2.4. *Pressure instrumentation*

Mean wall-pressures were measured using 24 1/4 mm diameter pressure taps located on the floor and ceiling of the test section bounding the boundary-layer test wall. Taps

were located in rows between 0.25 and 0.36 m away from the test wall. Mean pressure data were collected using an Esterline NetScanner Model 98RK pressure scanner.

Surface-pressure fluctuations were measured using an array of five Bruel and Kjaer type 4138-A-015 1/8 in. microphones fitted with 1/2 mm pinhole caps. Devenport *et al.* (2011) studied the effects of pinhole size on wall-pressure fluctuations measured under a wall-jet boundary layer and found that a 1/2 mm pinhole was sufficient to spatially resolve pressure fluctuations within 1 to 2 dB for boundary-layer edge velocities down to well below 20 m s^{-1}, the lowest speed used in the present study. A sixth B&K 4138 microphone, with a factory-provided salt and pepper cap, was used to sense the low-frequency acoustic background of the wind tunnel so it could be identified and eliminated from the signals of the other sensors.

Microphones were mounted with their caps flush (to within ± 0.02 mm) with either the smooth wall or the substrate of each rough surface. Given Varano's (2010) observations, microphones were placed as far as possible from adjacent roughness elements. For the ordered surfaces most microphone locations were therefore at the centre of a cell of four elements. The random surface design was initially selected from a number of statistically identical designs so as to avoid direct conflict between the planned microphone locations and the roughness elements. Microphones were mounted in plastic sleeves that allowed easy removal and replacement in the test wall. This allowed repeated measurements of the same flow with different microphone configurations. Microphone power, signal conditioning and data acquisition were handled using B&K Type 3050-A-060 LAN XI models which provided 24-bit simultaneous sampling at 51.2 kHz. The amplitude gain of the microphones was calibrated daily using a B&K type 4228 Pistonphone operating at 250 Hz.

Amplitude and phase response of the B&K type 4138 microphones fitted with pinholes was determined using an unaltered model 4138 microphone as a reference. Calibrations were performed in an anechoic chamber using the Agilent E1432 digitizer to generate white noise through a University Sound ID60C8 speaker. The pinhole cap produced a resonant peak in the microphone response at around 15 kHz which produced amplitude and phase variations that could be accurately fitted to the transfer function of a simple second-order system. Subsequent tests in the wind tunnel showed the shape of the resonant peak to depend on flow speed. Specifically, it was found that the damping of the response decreases with increase in Reynolds number, as the relative magnitude of the viscous effects is reduced. Microphone calibrations were therefore optimized during post-processing to account for these effects. Only adjustments to the damping were significant and then only at flow speeds above 20 m s^{-1}, the largest reductions being approximately 40 % at 60 m s^{-1}.

3. Results and discussion

3.1. *Mean pressure and velocity measurements*

Measurements were made at free-stream velocities of 30 and 60 m s^{-1}. Figure 4 shows the mean pressure coefficient as a function of streamwise distance x for each of the different surface conditions. For all wall conditions there are slight residual favourable streamwise pressure gradients acting on the flow. The average gradient is smallest for the smooth wall, 1 mm ordered roughness and 3 mm random roughness conditions at approximately -0.005 m^{-1}, and strongest for the 3 mm ordered roughness cases, at approximately double this value. The implied accelerations are mild (with $7 \times 10^{-10} < -(\nu/U_e^2)(\mathrm{d}U_e/\mathrm{d}x) < 3 \times 10^{-9}$) but not negligible as will be discussed below.

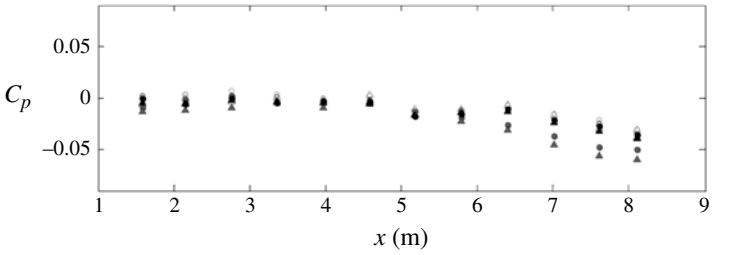

FIGURE 4. Mean pressure coefficient variation along the test wall. Smooth wall: ○, $U_e =$ 30 m s^{-1}; △, 60 m s^{-1}. 1 mm ordered roughness: ○, 30 m s^{-1}; △, 60 m s^{-1}. 3 mm ordered roughness: ●, 30 m s^{-1}; ▲, 60 m s^{-1}. 3 mm random roughness: ●, 30 m s^{-1}; ▲, 60 m s^{-1}.

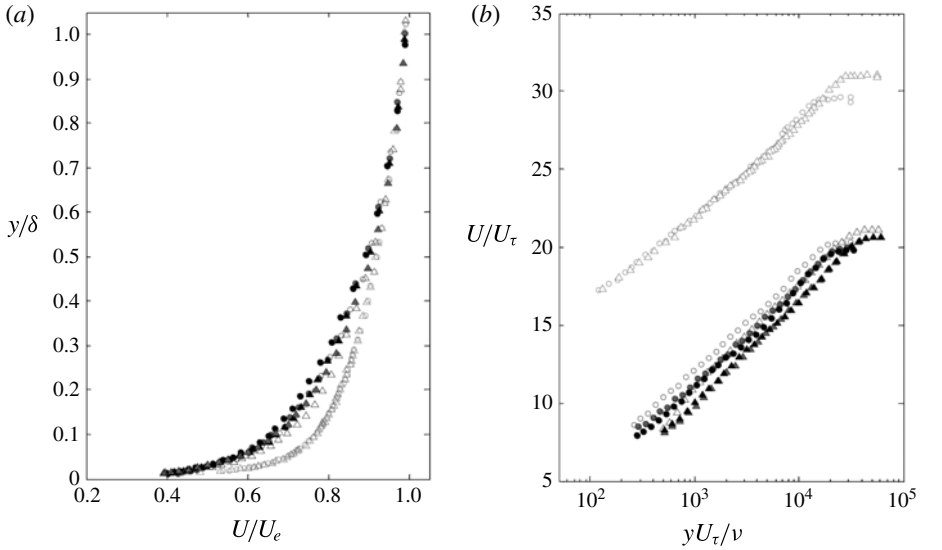

FIGURE 5. Mean velocity profiles, normalized on outer scales (*a*) and inner scales (*b*). See figure 4 for symbol definitions.

Mean velocity and turbulence profiles were measured for all cases at $x = 6.98$ m, close to the centrespan of the wall ($z = 0$). Exact spanwise locations were adjusted by a few millimetres so as to place the probes as far as possible from nearby roughness elements and avoid local element effects. With the smooth wall, mean velocity profiles measured at $z = \pm 0.153$ and ± 0.457 m were found to be almost identical to those measured at the centreline, establishing the mean two-dimensionality of the flow. A similar check on the two-dimensionality was made by examining mean velocity profiles at $x = 4.7$ m, see Forest (2012) and Meyers (2014) for details.

Mean velocity profiles measured for the four surface conditions at two speeds, at $x = 6.98$ m, are compared in figure 5. Boundary-layer parameters determined from the mean velocity profiles are listed in table 2. The smooth wall produces a 231 mm thick boundary layer with an extensive semi-logarithmic region and momentum thickness Reynolds numbers of 35 700 and 68 700 at 30 and 60 m s^{-1}. The addition of roughness, of course, increases the velocity defect near the wall and shifts the

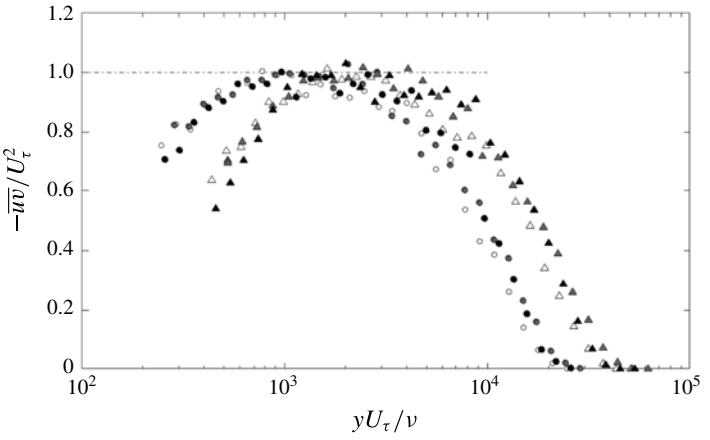

FIGURE 6. Reynolds shear stress profiles for the rough-wall boundary layers normalized on the friction velocity. See figure 4 for symbol definitions.

profile downward on the semi-logarithmic scale of figure 5(*b*). Interestingly, the defect is only slightly greater with the 3 mm than the 1 mm roughness, and the mean velocity profiles appear almost identical for the random and ordered 3 mm surfaces. Adding roughness to the flow surface caused a slight reduction in the boundary-layer thickness measured at $x = 6.98$ m (see table 2), probably reflecting a shift in the virtual origin of the boundary layer. Boundary-layer thicknesses only show slight changes with flow speed. The outer portion of the boundary-layer profiles show a somewhat weaker wake region than other measurements at high Reynolds numbers. This is a well-known effect of a favourable streamwise pressure gradient that appears even when that gradient is mild (Oweis *et al.* 2010), as in the present flows.

Skin friction coefficients for the flows were determined using the same profile-fitting method as employed by Blake (1970) and Aupperle & Lambert (1970) and detailed by Schlichting (1979). This involves a two-parameter optimization of the friction velocity U_τ and the equivalent sand-grain roughness k_s achieved by fitting the mean velocity profile to the form

$$\frac{U}{U_\tau} = \frac{1}{\kappa}\ln\left(\frac{yU_\tau}{\nu}\right) - \frac{1}{\kappa}\ln\left(\frac{k_s U_\tau}{\nu}\right) + C \tag{3.1}$$

with $C = 8.5$. The friction velocity estimates (listed in table 2) are verified in figure 6, which shows the independently measured Reynolds shear stress profiles normalized on these estimates. As would be expected, the peak values of $-\overline{uv}/U_\tau^2$ are all one, to within the scatter of the measurement.

Examining the results in table 2 we see that friction velocity ratios U_τ/U_e are approximately 50 % larger for the rough surfaces and almost identical for the random and ordered 3 mm hemispheres. The friction velocities imply roughness Reynolds numbers (k_g^+) that, according to conventional criteria, suggest fully rough flows in all cases; k_g^+ varies from 91 for the 1 mm surface at 30 m s^{-1} to 507 for the 3 mm ordered surface at 60 m s^{-1}. Consistent with this, the effective sand-grain roughness is a nearly constant multiple of the geometric roughness height. Boundary-layer

https://doi.org/10.1017/jfm.2014.743 Published online by Cambridge University Press

Surface	U_e (m s^{-1})	δ (mm)	δ^* (mm)	Re_θ	k_g (mm)	k_s (mm)	λ	k_g^+	k_s^+	δ/k_g	δ^+	ΔU^+	U_τ/U_e
Smooth	30	231	24.6	35 700	—	—	—	—	—	—	16 000	—	0.0338
1 mm ordered	30	212	29.6	39 600	1	1.12	0.052	91	102	212	19 200	9.2	0.0492
3 mm ordered	30	219	32.1	43 500	3	3.33	0.052	283	315	73	21 600	9.6	0.0501
3 mm random	30	222	33.6	45 200	3	3.33	0.052	260	289	74	19 300	9.7	0.0503
Smooth	60	231	24.9	68 700	—	—	—	—	—	—	29 300	—	0.0318
1 mm ordered	60	210	27.2	72 100	1	1.13	0.052	172	195	210	36 200	10.4	0.0474
3 mm ordered	60	228	31.9	80 200	3	3.35	0.052	507	566	76	42 500	11.2	0.0484
3 mm random	60	220	31.0	82 700	3	3.34	0.052	492	548	73	36 100	11.2	0.0484

TABLE 2. Boundary-layer parameters for the smooth and hemispherical rough surfaces at $x = 7$ m.

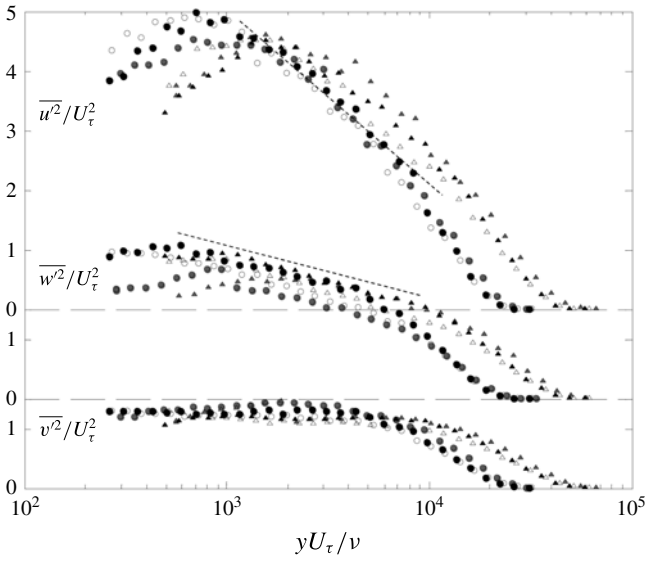

FIGURE 7. Reynolds normal stress profiles. See figure 4 for symbol definitions. Note false origins for $\overline{w'^2}$ and $\overline{u'^2}$. Dashed line on the $\overline{u'^2}$ profiles has a slope, in terms of the natural logarithm of y^+ of -1.26. Dashed line over the $\overline{w'^2}$ profiles has 30 % of this slope, matching the semi-logarithmic region seen by Fernholz & Finley (1996).

thickness to roughness size ratios vary from the mid-70s for the 3 mm surfaces to over 200 for the 1 mm roughness cases. All the present rough-wall flows, therefore, reach conditions at which we might expect universal scaling behaviour to become apparent.

As already noted, a complicating factor in the concept of fully rough conditions is Mehdi *et al.*'s (2010, 2013) argument that viscous effects should play a significant role in the boundary layer from the wall out to the Reynolds shear stress maximum. As seen in figure 6, the Reynolds stress maxima all appear well above the roughness tops, at a roughly constant absolute position of $y \cong 11$ mm, corresponding to $y/\delta \cong 5\,\%$ and $y^+ \cong 1000$ and 2000 at the two flow speeds. Note that this distance is comparable to the roughness spacings (of 5.5 and 16.5 mm), so the local flows around the elements may also have influenced the lower portions of the profiles, which were deliberately measured over the gaps between roughness elements.

Turbulence normal stress profiles, plotted in semi-logarithmic form, are shown for the rough-wall boundary layer cases in figure 7. The profiles show the expected dominance of u' velocity fluctuations over most of the boundary layer and the suppressed level of v' fluctuations due to the non-penetration condition at the wall. Meyers (2014) shows that peak turbulence levels in the boundary layer are quite similar to those of Blake (1970) although those profiles, measured at significantly lower Reynolds numbers, have higher turbulence levels in the outer region. While there is some uncertainty in the $\overline{u'^2}$ data, these profiles have a variation in the outer part of the boundary layer not inconsistent with the semi-logarithmic region seen in other high-Reynolds-number boundary-layer measurements, with a natural-logarithm slope of -1.26. This is the value established by recent smooth-wall studies of Marusic *et al.* (2013) and Meneveau & Marusic (2013). The $\overline{w'^2}$ profiles display a somewhat clearer semi-logarithmic region with a slope quite closely consistent with the highest

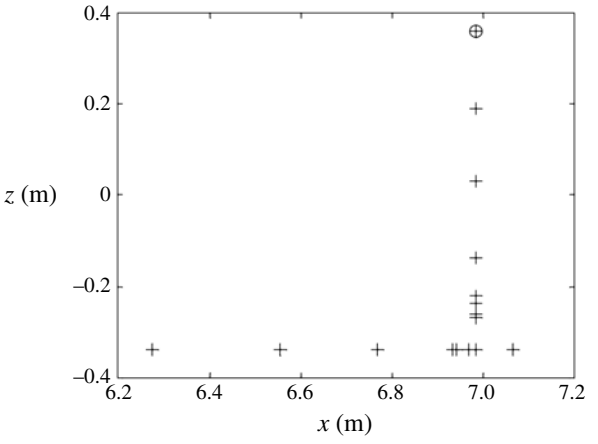

FIGURE 8. Microphone measurement locations. Location of the reference microphone used for acoustic background detection is indicated by the circle.

Reynolds number measurements of Fernholz & Finley (1996), for a boundary layer at $Re_\theta = 4736$ and a number of other smooth-wall datasets reviewed by Jiménez & Hoyas (2008).

Spatial resolution of the four-sensor hot-wire probe is an important consideration in interpreting the turbulent stress results. Based on the standard established by a number of previous studies (e.g. Hutchins *et al.* 2009) for the resolution of the nearest wall structure of smooth-wall boundary layers the present measurements are unquestionably under-resolved. The sensor lengths and separations in the four-sensor probes correspond to approximately 70 and 140 wall units at 30 and 60 m s^{-1}, much larger than the value of 20 normally quoted as necessary for near-wall turbulence (Ligrani & Bradshaw 1987). However, our goal here was merely to reveal the outer form of the stress profiles including the anticipated plateau in the Reynolds shear stress. Varano (2010) performed an exhaustive study of skin-friction measurement methods for rough-wall turbulent boundary layers and found the measurement of the Reynolds shear stress in the plateau to be particularly accurate. The present measurements were performed starting at 3 mm from the wall, a y^+ of close to 280 and 510 at 30 and 60 m s^{-1} respectively. The four-sensor probe measurements of Wittmer *et al.* (1998) in a fully developed pipe flow with quite similar absolute conditions to the present 30 m s^{-1} experiments showed under-measurements of the Reynolds shear stress of 8 %, 4 % and 1 % at $y^+ = 300$, 450 and 600 respectively, these last two values being smaller than the likely measurement uncertainty. If we assume this error scales with the size of the sensor, in wall units, then we would expect these errors to apply at roughly twice the y^+ values for the 60 m s^{-1} cases. These errors seem likely to emphasize the roll off in the Reynolds shear stress at the lower end of the y^+ range in figure 6, but unlikely to influence the peak value and its location. We can assess the influence of probe resolution on the normal stresses using the results of Hutchins *et al.* (2009) made for a single-sensor probe. They found that sensor lengths of 79 and 153 produced under-measurement of the streamwise turbulence normal stress in the outer portions of a turbulent boundary layer at $y^+ = 280$ of approximately 6 % and 1.5 %, respectively, and at $y^+ = 540$ of approximately 3 % and 1.2 %, respectively. These errors should be borne in mind when interpreting the left-most portions of the profiles in figures 6 and 7.

3.2. *Wall-pressure spectra*

Microphone measurements were made at a series of positions defining streamwise and spanwise lines around $x = 7$ m, as illustrated in figure 8. Measurements were made at multiple positions to verify the homogeneity of the wall pressure field, to define streamwise and spanwise separations for the measurement of space–time correlations and, through averaging, to reduce the uncertainty in wall-pressure time spectra. Two-point correlation results, discussed in more detail by Forest (2012) and Meyers (2014), show the correlation between boundary-layer pressure fluctuations falling to zero for spanwise separations of more than a few displacement thicknesses. Turbulent pressure fluctuations measured at the reference microphone location (marked as ○ in figure 8) were therefore independent of those measured at other microphone positions. Surface-pressure cross-spectra with the reference microphone could therefore be used to provide a measurement of the acoustic contribution to spectral levels. Significant acoustic contamination was only observed below 100 Hz, with broadband contamination not exceeding 3 dB for frequencies above 12 Hz. At frequencies where the acoustic contribution was a small fraction of the measured levels it was subtracted from those levels. Data at frequencies where the coherence between the measurement and reference microphone exceeded 0.08 were discarded.

Wall-pressure fluctuations for all the rough-surface conditions were measured at flow speeds of 20, 30, 40, 50 and 60 m s^{-1}. The smooth-wall measurements were made at 22.4, 33.6, 44.8, 56.0 and 67.2 m s^{-1}, the inadvertent difference being due to a mis-connected pressure transducer. Figure 9 shows absolute surface-pressure spectra measured at these conditions. Spectra are single sided and scaled to a 1 Hz bandwidth and are shown using multiple curves representing different locations along the spanwise row at $x = 6.98$ m.

The results for the smooth wall (figure 9*a*) display traits typical of wall-pressure spectra observed in other zero-pressure-gradient turbulent boundary-layer flows. A low signal to noise ratio limited the data at very low frequencies, though there is clear evidence of a low frequency rise for each of the spectra before reaching a shallow maximum. In the mid-frequency range after the spectral peak, a well-defined linear 'overlap' region is exhibited before the wall-pressure spectra begin their sharp roll-off at high frequencies due to dissipation. Data acquisition system limitations restricted the Nyquist frequency to 25.6 kHz, causing clipping of the spectral roll-off for flow speeds above 20 m s^{-1}. Consistent with many previous studies (e.g. Blake 1970; McGrath & Simpson 1987; Goody 2004) the so-called overlap region has a slope of approximately -0.8 and grows in frequency span as the flow speed increases. It is commonly assumed that the low slope is a transitional effect, resulting from the relatively low Reynolds number of many laboratory-scale flows. However, the high Reynolds number of the present experiments suggests that either the theoretical argument for the -1 slope is flawed, or the convergence to this value at high Reynolds number is extremely gradual. In the dissipation range, the spectra roll off with a slope that appears to increases rapidly with frequency. At 20 and 30 m s^{-1} enough of this region is visible to see that the slope reaches, and then exceeds, the commonly stated value of -5. While this type of behaviour has been seen before, both in experimental (e.g. Tsuji *et al.* 2007) and computational (Choi & Moin 1990) studies, the increasingly rapid roll off here appears due to averaging effects over the microphone pinhole, as will be discussed below. As the flow speed and Reynolds number are increased, a shallow inflection appears between the 'overlap' and dissipation ranges, somewhat reminiscent of the bottleneck observed in the energy spectrum of homogeneous turbulence.

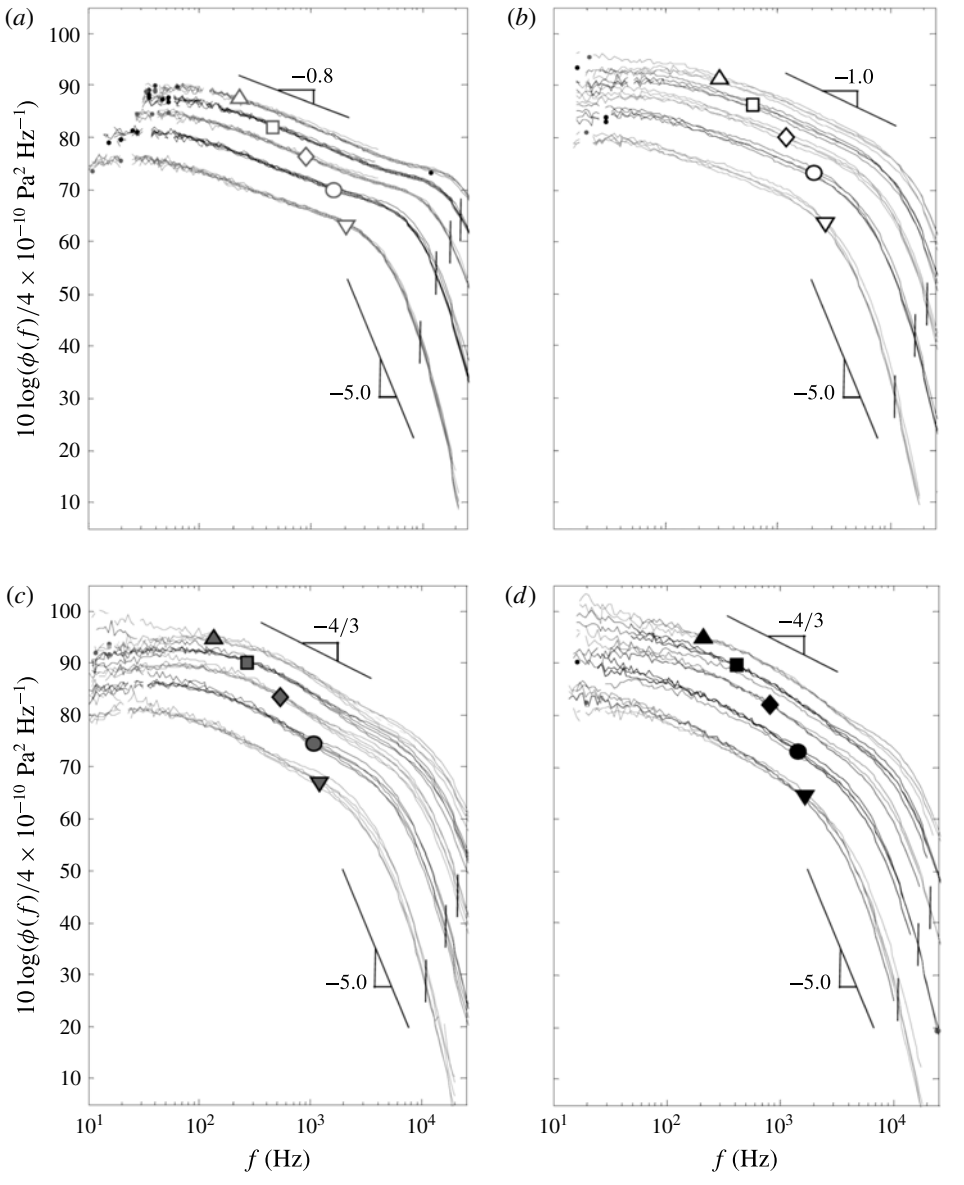

FIGURE 9. Pressure spectra measured at different spanwise positions at $x = 6.98$ m. (*a*) Smooth wall: ▽, U_e = 22.4 m s^{-1}; ○, 33.6 m s^{-1}; ◇, 44.8 m s^{-1}; □, 56 m s^{-1}; △, 67.2 m s^{-1}. (*b*) 1 mm ordered surface: ▽, $U_e = 20$ m s^{-1}; ○, 30 m s^{-1}; ◇, 40 m s^{-1}; □, 50 m s^{-1}; △, 60 m s^{-1}. (*c*) 3 mm ordered surface: ▼, $U_e = 20$ m s^{-1}; ●, 30 m s^{-1}; ◆, 40 m s^{-1}; ■, 50 m s^{-1}; ▲, 60 m s^{-1}. (*d*) 3 mm random surface: ▼, $U_e = 20$ m s^{-1}; ●, m s^{-1}; ◆, 40 m s^{-1}; ■, 50 m s^{-1}; ▲, 60 m s^{-1}. Vertical lines through the spectra at high frequency indicate, in each case, the frequency above which attenuation due to averaging over the pinhole would have been significant.

The pressure spectra on the rough walls have a superficially similar form to those measured on the smooth wall: a shallow maximum at low frequencies (that appears obscured by uncertainty for the 3 mm random surface), a mid-frequency

region of roughly constant slope, and a rapid roll off at high frequencies with a slope that passes through and beyond -5. However, a detailed comparison reveals some important differences. The spectral maximum appears at a higher absolute frequency for the same free-stream speed and, comparing the results for the 1 mm and 3 mm ordered surfaces, its frequency clearly increases with the roughness size. The mid-frequency region is less convincingly straight than with the smooth wall and has a noticeably higher slope, of approximately -0.9 for the 1 mm hemispherical roughness, and $-4/3$ for both 3 mm surfaces.

We would expect any effects of the slight favourable pressure gradient of the present flows on the spectrum to be most noticeable at lower frequencies where the wall-pressure spectrum contains its strongest contributions from the outer portion of the turbulent boundary layer. Schloemer (1967) made measurements of the effects of favourable pressure gradient on the wall-pressure fluctuations of a smooth-wall boundary layer for an acceleration parameter $K = 3.3 \times 10^{-7}$ more than two orders of magnitude greater than those of the present flows. Schloemer's data were further analysed by Cipolla & Keith (2000) who found that, when scaled on outer variables, the wall-pressure fluctuations in the favourable-pressure-gradient boundary layer were suppressed at frequencies $\omega\delta/U_e \lesssim 3$, corresponding to dimensional frequencies in the present flows of approximately 40 Hz at 20 m s^{-1} increasing to approximately 130 Hz at 60 m s^{-1}. This encompasses the region in the immediate vicinity of the low-pressure maximum. This could explain, at least for the smooth-wall case, why the roll off from the maximum is rounded and involves a continuous increase in slope magnitude with frequency. Pressure spectra measured by some authors (e.g. Klewicki *et al.* 2008) show a more pronounced maximum that is also present in Panton & Linebarger's (1974) smooth-wall spectral model. However, this feature does not appear to be universal to smooth-wall boundary layers as can be seen in the data sets reviewed by Goody (2004) and, indeed, Goody's model does not include this feature.

A close examination of the results for the 3 mm ordered and random rough surfaces (figure 9*c*,*d*) show them to be nearly identical in all significant details. An overlaid comparison of streamwise-averaged spectra show differences of 2 dB or less in the spectral level at 20 m s^{-1}, with pressure fluctuations for the random distribution of roughness elements generally being weakest. This difference disappears as the flow speed is increased.

The spanwise uniformity of the pressure fluctuation field, as revealed by the spread of the curves shown at each flow speed in figure 9, appears quite good for the smooth-wall flow. With the roughness, there is more variation at higher frequencies, presumably because of slight differences in the effects of local roughness elements. Pressure spectra measured at different streamwise positions in the array show a comparable level of similarity, suggesting near homogeneous flow in planes parallel to the wall. Therefore, wall-pressure spectra presented in later sections are averaged across the microphone locations.

It is well known that the finite size of a microphone pinhole can have a significant impact on the measurement of the highest-frequency pressure fluctuations. Perhaps the most definitive studies are those due to Schewe (1983) and Gravante *et al.* (1998). Schewe examined pressure fluctuations under a turbulent boundary layer using five microphones with pinholes with diameters d between 1 and 18 mm ($d^+ = dU_\tau/\nu = 19$–333). He concluded that a diameter of no more that $d^+ = 20$ was needed to completely resolve the pressure fluctuations, though his data showed that results from larger pinholes could be corrected using the method of Corcos (1963,

	Smooth-wall case		Rough-wall cases	
U_e (m s^{-1})	d^+	f_{max} (kHz)	d^+	f_{max} (kHz)
20	21	9.4	27	11
30	31	14	41	16
40	40	18	55	22
50	49	22	68	27
60	58	26	82	33

TABLE 3. Diameter of the 0.5 mm microphone pinhole expressed in wall units, and frequency limits on wall-pressure fluctuation measurements estimated using the results of Schewe (1983) and Gravante *et al.* (1998).

1967), to some extent. Gravante *et al.* (1998) performed a similar study but with a set of smaller microphones of $d^+ = 4$–27. They conclude that having $d^+ \leqslant 18$ avoids spectral attenuation for frequencies up to $f^+ = f\nu/U_\tau^2 = 1$.

Schewe (1983) and Gravante *et al.* (1998) achieved the low values of d^+ they needed in part by studying slow-speed flows (16 m s^{-1} or less) where the viscous scale is large. At the higher speeds demanded by the requirements of high Reynolds number, achieving such d^+ values implies pinhole diameters that (at least with the present microphones) would be incompatible with maintaining a sufficient frequency response. The present microphone system therefore under-resolves the highest-frequency pressure fluctuations. However, we can use the results of Gravante *et al.* (1998) and Schewe (1983) to estimate the frequencies at which that attenuation would have become significant. Table 3 lists d^+ for the 0.5 mm pinholes used in the present experiments as functions of flow speed and surface. Gravante *et al.*'s (1998) results include a case, with $d^+ \approx 26$, where the pressure spectrum was under-resolved. In this case the measured spectral levels were within 2 dB of the true levels up to a frequency $f^+ \approx 2.2$. We can use this result to estimate the maximum useful frequency measured by the current microphones by assuming that this frequency varies inversely with d^+. If anything, Schewe's (1983) results, which include a sequence of spectra measured with increasingly under-resolved transducers, suggest that this is a pessimistic estimate. High-frequency limits on the present measurements estimated using this method are included in table 3 and shown graphically with the vertical lines in figure 9. These limiting frequencies lie only within the measured frequency range (up to 25 kHz) at flow speeds of 30 m s^{-1} or less (40 m s^{-1} for the smooth wall). At these speeds the limits come in the middle of the dissipation range and largely clip the portion of the spectrum that rolls off with a slope greater than -5, at least for the smooth wall condition. Data above the limiting frequencies are not included in subsequent figures.

3.3. *Scaling of the pressure spectrum*

The applicability of various scaling suggestions made by previous researchers are examined in this section. We consider not only their applicability to the different rough-surface flows of the present experiments, but also the extent to which they correlate the present results to those of the previous studies listed in table 1, where the boundary layer to roughness size ratios were not as large, but which represent a range of sparseness ratios and roughness geometries.

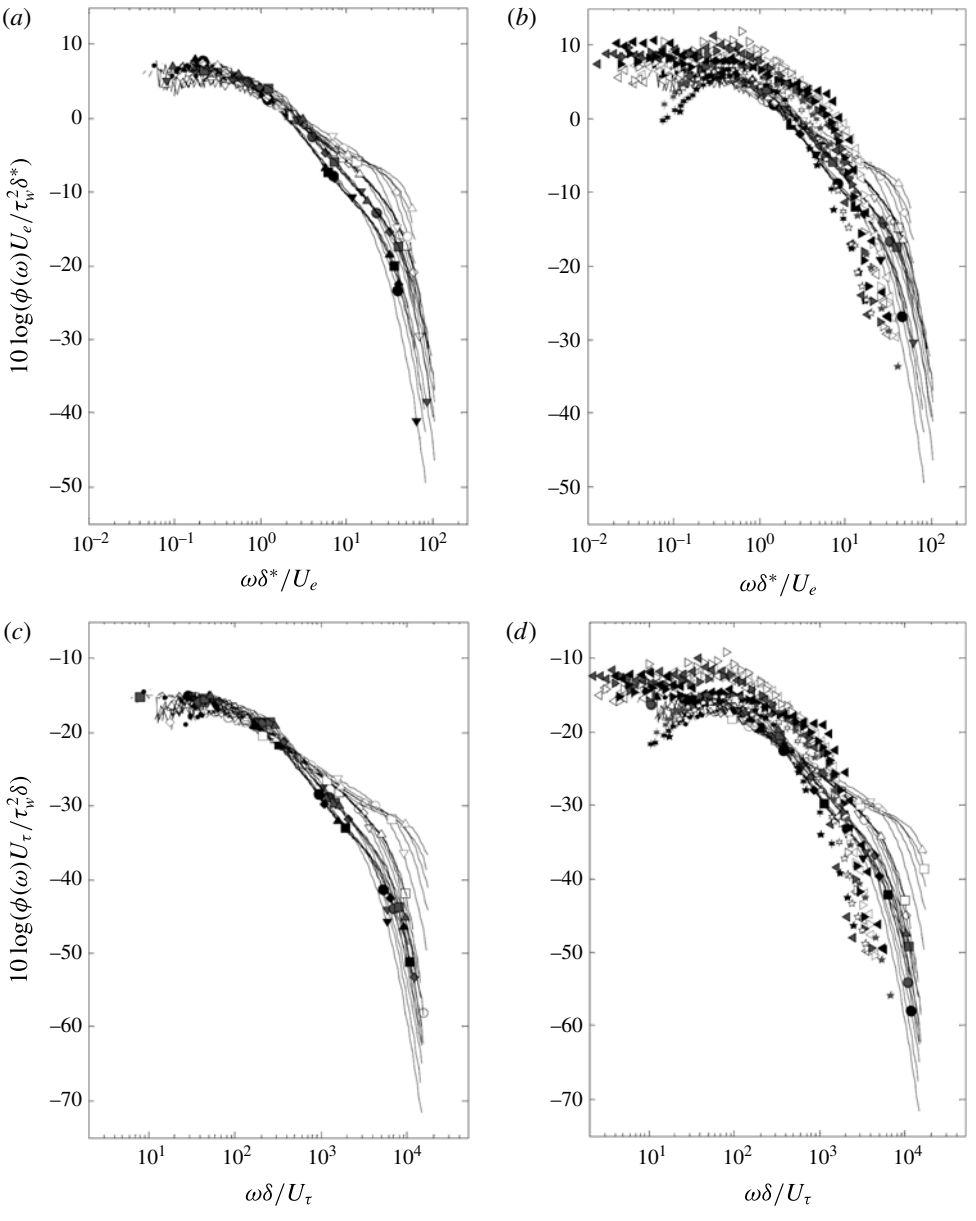

FIGURE 10. Pressure spectra measured scaled using outer variables. Mixed outer scaling, present data (*a*) and with results from prior studies (*b*). Classical outer scaling, present data (*c*) and with results from prior studies (*d*). Symbols for present data given in figure 4. ◁, Varano (2010) fetch 1, 27 m s^{-1}; ▷, 20 m s^{-1}; ◁, fetch 2, 27 m s^{-1}; ▷, 20 m s^{-1}; ◀, fetch 3, 27 m s^{-1}; ▶, 20 m s^{-1}; ◀, fetch 4, 27 m s^{-1}; ▶, 20 m s^{-1}; ★, Blake (1970) D-L, 38 m s^{-1}; ★, 50 m s^{-1}; ★ S–S, 38 m s^{-1}; ★, 50 m s^{-1}; ✯ D–S, 38 m s^{-1}; ✯, 50 m s^{-1}.

We begin with the low-frequency portion of the spectrum which is expected to scale on outer variables. Many different scalings were tried for this region, the best of which are shown in figure 10. Figure 10(*a*) shows the 'mixed' scaling used by

Blake (1970), $\phi(\omega)U_e/\tau_w^2\delta^*$ versus $\omega\delta^*/U_e$, applied to the present measurements. This scaling correlates all the spectra measured on the smooth and rough walls, and at different speeds, to within approximately ± 1.5 dB for frequencies up to $\omega\delta^*/U_e \approx 4$, well beyond the spectral peak. Adding the data from previous studies (excluding the data of Aupperle & Lambert 1970, which show no low-frequency maximum) results in a somewhat less convincing plot (figure 10*b*). Spectra still correlate best near the peak, but are spread over a band some 6–7 dB wide from $\omega\delta^*/U_e \approx 2$ to 4. However, approximately half of the scatter in this band is due to Varano's (2010) data, most of which lie above the present measurements, and those of Blake (1970), and do not collapse well within themselves when normalized in this way. Varano himself noted this lack of collapse at low frequency and attributed it to the merger of the outer portion of his boundary layer with the boundary layer growing on the opposite wall of the channel in which his experiments were performed.

Shown in figure 10(*c*,*d*) is the 'classical' low-frequency scaling used for smooth-wall boundary-layer pressure spectra by Farabee & Casarella (1991) and Goody (2004), $\phi(\omega)U_\tau/\tau_w^2\delta$ versus $\omega\delta/U_\tau$. This produces almost identical results to those of the mixed scaling, closely correlating the low-frequency portions of the present smooth- and rough-wall pressure spectra approximately in the range $20 \lesssim \omega\delta U_\tau \lesssim 800$ (figure 10*c*). We see in figure 10(*d*) that this scaling also does quite well in correlating the present low-frequency results to those of Blake (1970) but, as with the mixed scaling, leaves Varano's data above these data sets. Even though the mixed and classical outer scalings perform comparably, we believe that the classical scaling should be preferred since it is more fundamental and physically justifiable, depending on a distance scale (δ) directly experienced by the flow rather than one implied by its mean profile. We therefore conclude that, of the normalizations considered, the classical scaling is most likely to describe the low-frequency behaviour of rough-wall turbulent boundary-layer pressure spectra.

Other low-frequency scalings attempted included normalizing the spectra using only boundary-layer edge scales, i.e. $\phi(\omega)U_e/(\rho U_e^2)^2\delta$ versus $\omega\delta/U_e$. This was found to better align the low-frequency portions of Varano's (2010) spectra with the other rough-wall data but displaces all the rough-wall results approximately 8 dB above those for smooth walls in this range, a result incompatible with the expectation that the true low-frequency scaling should unite the low-frequency behaviour of both smooth- and rough-wall boundary layers. A similar result (collapse of the low-frequency portions of the smooth and rough-wall spectra onto different curves) was seen with the normalization $\phi(\omega)U_e/(\rho U_e U_\tau)^2\delta$ versus $\omega\delta/U_e$ inspired by DeGraaff & Eaton's (2000) scaling for streamwise velocity fluctuations in smooth-wall boundary layers at high Reynolds numbers. Normalizations were also constructed using the hybrid scale $\sqrt{\delta\nu/U_\tau}$ discussed by Klewicki *et al.* (2009) and associated with the pressure-centre of (smooth-wall) boundary layers. Despite its uncertain applicability to rough-wall flows, using this in place of δ in the classical scaling produced a collapse of the present rough-wall spectra with those of Blake (1970) and Varano (2010) slightly better than that achieved with the mixed scaling (figure 10*a*). However, correlation between rough- and smooth-wall flows was not quite as good as with the mixed or classical scalings.

We now turn our attention to examining the so-called 'inner scaling' for the rough-wall data. Blake (1970) first argued that the pressure fluctuations generated from the inner portion of the boundary layer should scale as $\phi(\omega)U_\tau/(\tau_w^2 k_g)$ versus $\omega k_g/U_\tau$ at high frequency. Note that the frequency scale $\omega k_g/U_\tau$ is essentially the roughness Strouhal number. Aupperle & Lambert (1970) considered a similar scaling using the

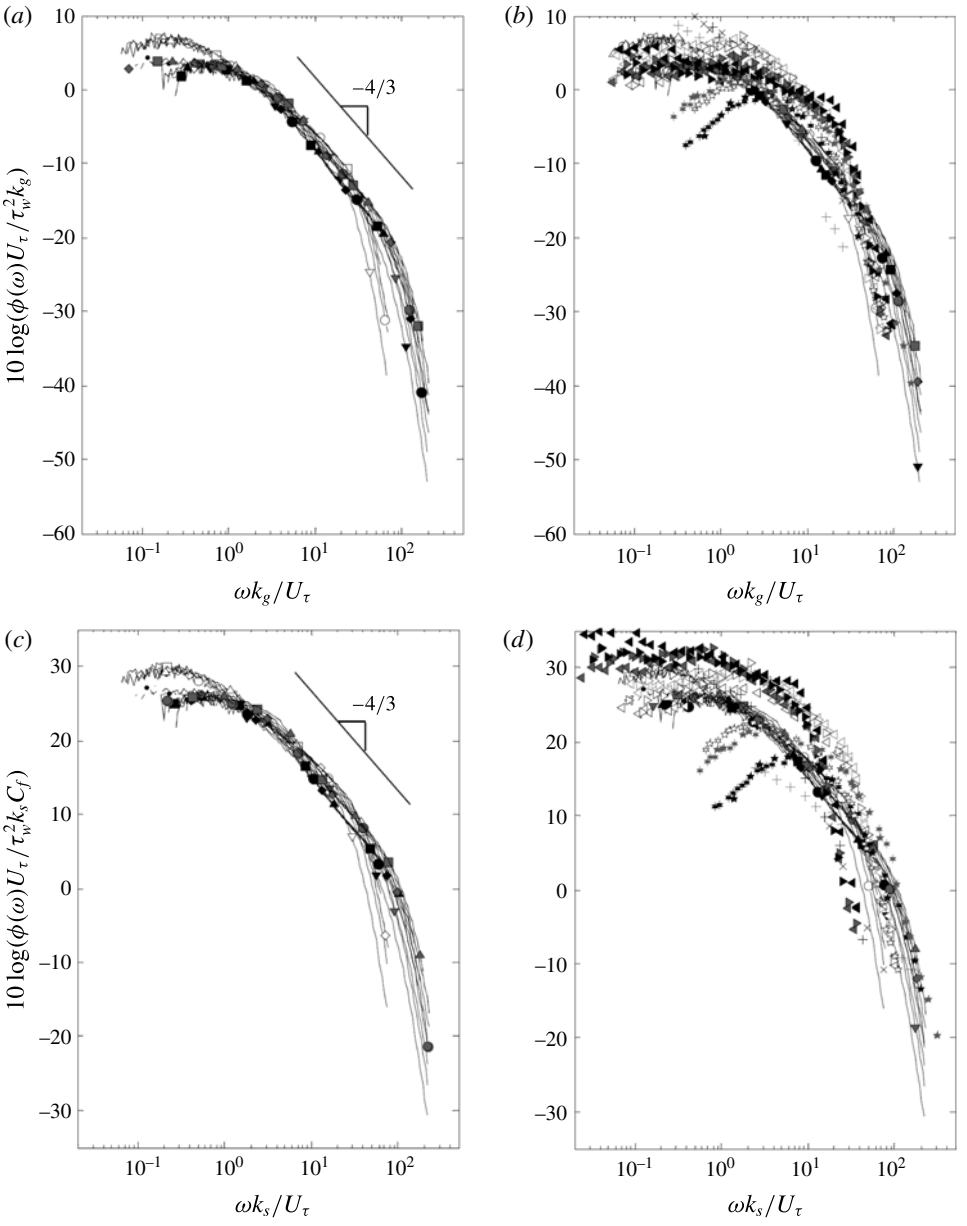

FIGURE 11. Pressure spectra scaled using previously proposed inner-variable scalings. Blake scaling, present data (*a*) and with results from prior studies (*b*). Aupperle and Lambert scaling, present data (*c*) and with results from prior studies (*d*). Aupperle and Lambert; +, grade 36; ×, grade 12; +, grade 4. Other symbols given in figure 10.

effective sand-grain roughness height k_s instead of k_g, and with the spectral level additionally normalized on C_f, i.e. $\phi(\omega)U_\tau/\tau_w^2 k_s C_f$ versus $\omega k_s/U_\tau$.

Figure 11(*a*) depicts Blake's scaling using data from the present study. This clearly does not collapse the highest-frequency portions of the pressure spectra as there is a vast variation here across test speeds and configurations. Figure 11(*b*) shows the

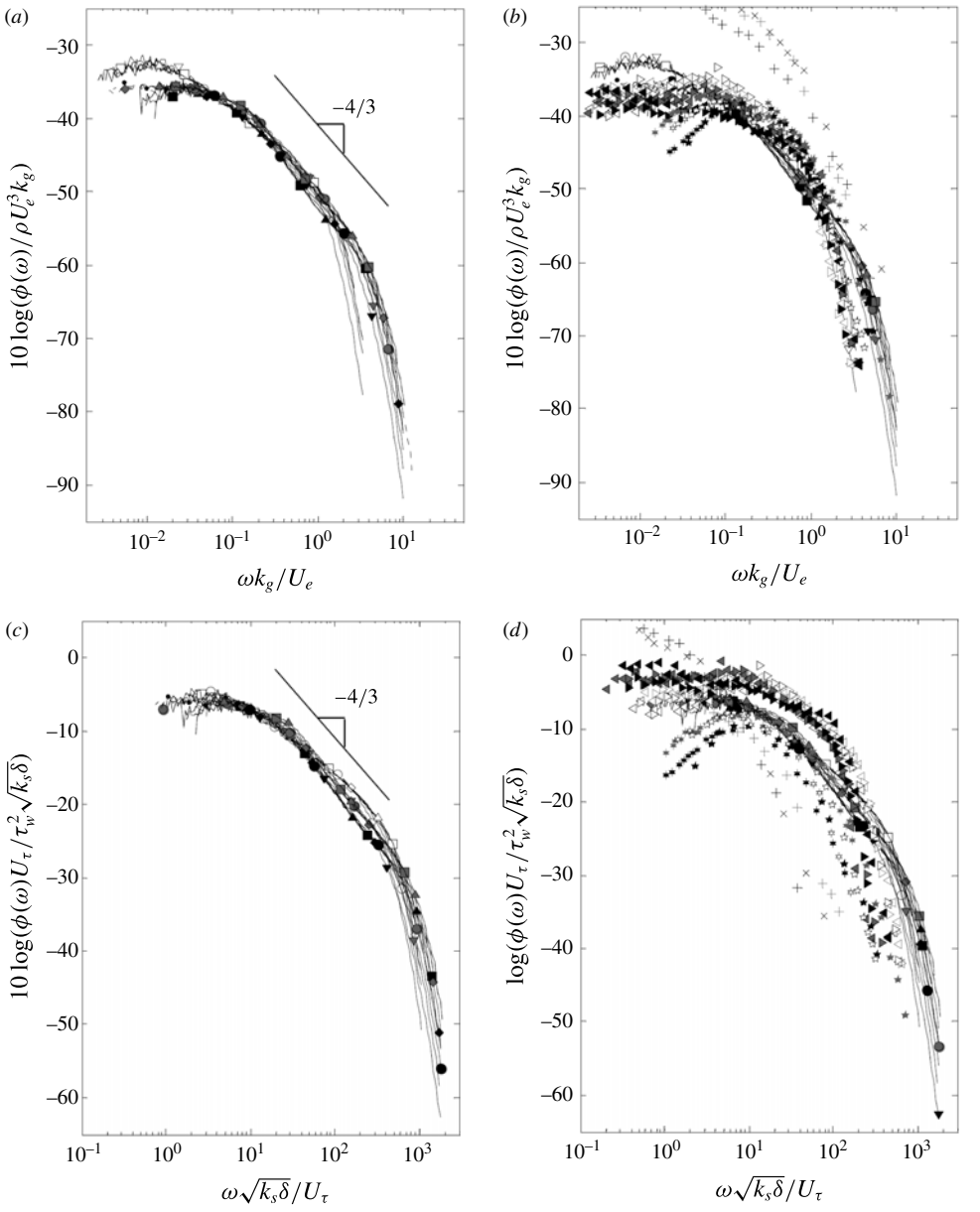

FIGURE 12. Pressure spectra scaled using roughness scalings. Varano scaling, present data (*a*) and with results from prior studies (*b*). Scaling based on Mehdi *et al.*'s (2013) hybrid roughness/boundary layer thickness scale $\sqrt{k_s\delta}$, present data (*c*) and with results from prior studies (*d*). Symbols given in figure 11.

same data with the added studies of Aupperle & Lambert (1970), Blake (1970) and Varano (2010). Similar lack of performance is seen with Aupperle & Lambert's scaling applied to data from the present study in figure 11(*c*), and to all the data sets in figure 11(*d*).

Although Blake's scaling fails at the highest frequencies, it does show some clear signs of collapsing the spectra in the mid-frequencies $3 < \omega k_g/U_\tau < 20$ where it aligns the spectra so that they group into a single narrower band whose overall slope is around $-4/3$. Looking at just the present data, figure 11(*a*), which combine the largest roughness Reynolds numbers and largest boundary-layer thickness to roughness size ratios, the collapse is particularly good, and to within approximately ± 1 dB. The correlation using Blake's scaling is less clear when all the data sets are included as shown in figure 11(*b*), but is better than that produced by Aupperle & Lambert's scaling, see figure 11(*d*).

Recently Varano (2010) proposed another so-called inner variable scaling. Starting with Blake's scaling, Varano argued that for fully rough flows the friction velocity should be proportional to the edge velocity. If replaced, one obtains the scaling $\phi(\omega)/(\rho^2 U_e^3 k_g)$ versus $\omega k_g/U_e$. Varano's scaling is applied to the pressure spectra for the present study in figure 12(*a*). This scaling also fails at high frequencies but is perhaps the most successful in collapsing the mid-frequency region $0.06 < \omega k_g/U_e < 1$. Varano's scaling also produces the best mid-frequency correlation between the present data and the spectra of Blake and Varano, but is unable to scale Aupperle & Lambert's results, figure 12(*b*).

A number of normalizations derived from the distance scales for rough-wall boundary layers proposed by Mehdi *et al.* (2010) were considered. Figure 12(*c,d*) shows the scaling $\phi(\omega)U_\tau/\tau_w^2\sqrt{k_s\delta}$ versus $\omega\sqrt{k_s\delta}/U_\tau$, based on the hybrid roughness/boundary-layer thickness scale $\sqrt{k_s\delta}$. Looking only at the present data (figure 12*c*), this scaling appears to work particularly well at the low-frequency end of the $-4/3$ region and provides a measure of collapse around the spectral maximum, perhaps not surprising as it is the geometric average of the classical outer region and Blake scalings. This formulation does not do well in correlating the present results with other data sets, however, as shown in figure 12(*d*).

With the benefit of hindsight, it is perhaps not surprising that Blake's, Aupperle & Lambert's and Varano's scalings do not work at the highest frequencies since none of them contains any direct reference to viscosity. Even in a high-Reynolds-number rough-wall flow one would expect viscosity to ultimately control the smallest turbulent scales and thus the highest-frequency pressure fluctuations. Indeed, the discussion of Mehdi *et al.* (2010, 2013), referenced above, suggest that viscous effects may remain a substantial player in the dynamics of the near-wall region to a position well above the roughness tops, to the vicinity of the maximum in the Reynolds shear stress profile.

With the likely importance of viscosity to the high-frequency pressure fluctuations in mind, Forest (2012) postulated that a meshing of time scales was needed in order to scale the high-frequency pressure spectra. The scaling ν/u_τ^2 is based in the viscous time scale for the wall bounded flow, whereas Blake's scaling k_g/u_τ reflects the time scale for the roughness elements. Forest argued that even for fully rough flows, both time scales may still influence the near-wall turbulent structures. This led him to take the geometric average of both time scales, yielding a scaling of the form $\phi(\omega)U_\tau/\tau_w^2\sqrt{\nu k_g/U_\tau}$ versus $\omega\sqrt{\nu k_g/U_\tau}/U_\tau$, along with a similar scaling using the effective sand-grain roughness k_s. Mehdi *et al.* (2010) independently introduced the length scale $\sqrt{\nu k_s/U_\tau}$ as potentially important in describing the flow between the roughness tops and the Reynolds stress maximum. Figure 13(*a*) shows Forest's scaling applied to the data of the present study. It provides a marked improvement at the highest frequencies compared to the above formulations that do not include viscosity. However, it is unable to completely correlate the results for the 1 and

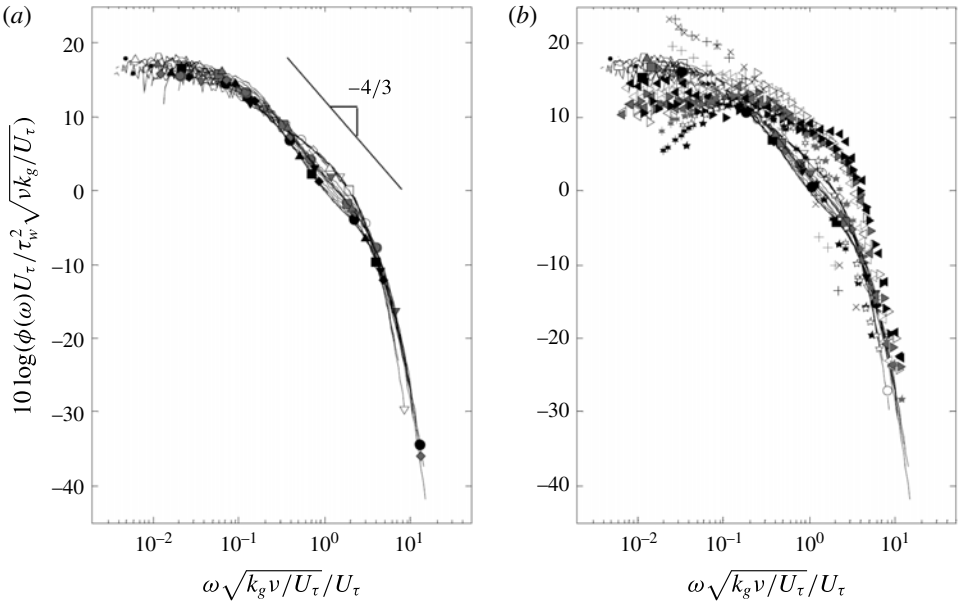

FIGURE 13. Pressure spectra normalized using Forest's (2012) scaling. Present data (*a*) and with results from prior studies (*b*). Symbols given in figure 11.

3 mm roughness cases, if only because the mid- and high-frequency portions of those spectra have different shapes. Adding the data from other studies produces the plot shown in figure 13(*b*). Overall Forest's (2012) formulation seems to provide the best compromise in scaling the right-hand portions of these spectra, given that the differing spectral shapes here preclude any exact single scaling. Note that using k_s in this scaling in place of k_g appeared to make no significance difference to the results.

3.4. *A new scaling for the highest-frequency pressure fluctuations*

In this section we address the possibility of scaling the highest-frequency portion of the pressure spectrum, namely the region of rapid rolloff where the slope of the spectrum is seen to reach −5. This region, clearly visible in the present measurements plotted in figure 9(*b–d*), bears more than a passing resemblance to the viscous dissipation region seen in the smooth-wall pressure spectra of figure 9(*a*). It is therefore tempting to suggest that both rough- and smooth-wall spectra follow a Kolmogorov-type scaling in this region. We therefore revisit the smooth-wall viscous scaling $\phi(\omega)U_\tau^2/(\tau_w^2\nu)$ versus $\omega\nu/U_\tau^2$, which is applied to the present rough- and smooth-wall data in figure 14(*a*). Normalized in this way, the high-frequency portions of the smooth-wall spectra collapse onto the same curve. The same is not seen for the rough-wall spectra, though, each of which roll off at widely separated normalized frequencies and levels. The rough-wall spectra are not totally unorganized, however, as the normalized roll off frequency is seen to increase consistently as the Reynolds number is reduced for each rough surface.

While the smooth-wall viscous scaling in its unmodified form does not come even close to collapsing the highest-frequency portion of the rough-wall pressure spectra, the viscous-like behaviour of this part of the spectrum leads us to propose a scaling of the form $\phi(\omega)U_v^2/(\tau_v^2\nu)$ versus $\omega\upsilon/U_v^2$, where U_v is a modified friction velocity

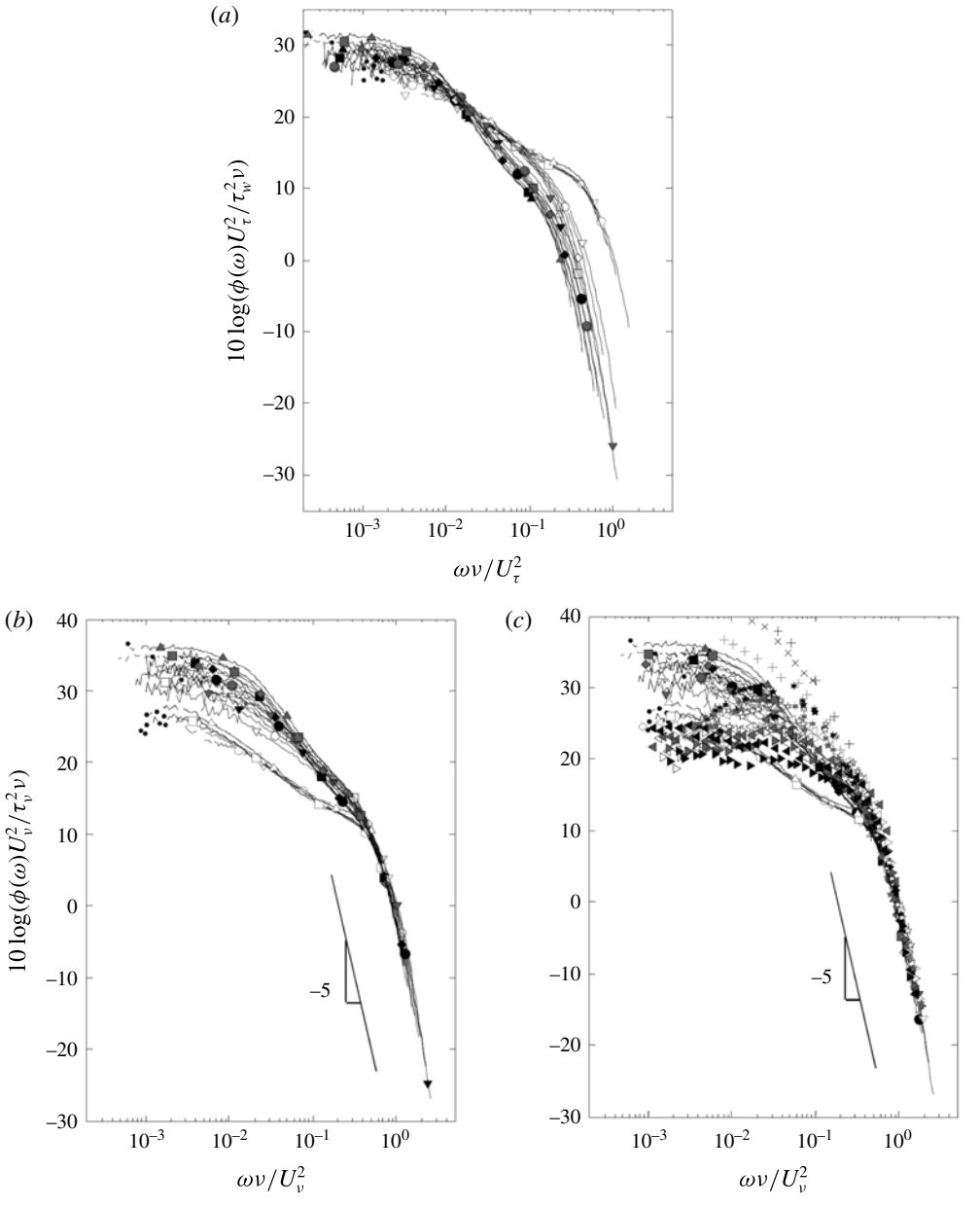

FIGURE 14. Pressure spectra scaled using viscous scales with (*a*) the conventionally defined friction velocity (present data), (*b*) the shear friction velocity (present data), and (*c*) the shear friction velocity (all datasets). Symbols given in figure 11.

and $\tau_\nu = U_\nu^2\rho$ is the corresponding wall shear stress. We will refer to U_ν as the 'shear friction velocity'. For a smooth wall we take U_ν as equal to the conventionally defined friction velocity. For a rough wall we choose the value of U_ν so that the high-frequency portion of the normalized spectrum matches that for the smooth wall, as nearly as possible. It is important to note that there is no *a priori* reason to believe

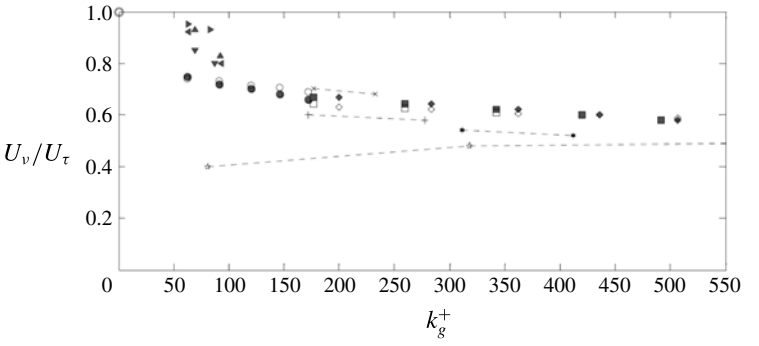

FIGURE 15. Shear friction velocities. Values inferred from pressure spectra: ●, 1 mm hemispheres; ◆, 3 mm hemispheres (ordered); ■, 3 mm hemispheres (random); ▼, Varano (2010), fetch 1; ▲, fetch 2; ◀, fetch 3; ▶, fetch 4; ×, Blake (1970) S–S; +, D–S; ✱, D–L; ✯, Aupperle & Lambert (1970). Open symbols for the present experiments show estimates obtained using (3.3).

that such a match can be made since the positioning of the scaled spectrum has two degrees of freedom, and the choice of U_v provides only one adjustment.

Nevertheless, it was found that values of U_v could be chosen to accurately collapse the high-frequency portions of all the current rough-wall pressure spectra as illustrated in figure 14(*b*). Using the same procedure it was found that values of U_v could be chosen for Varano's (2010), Blake's (1971) and Aupperle & Lambert's (1970) rough-wall pressure spectra that would likewise correlate the roll off regions. Figure 14(*c*) shows the resulting normalized spectra, all of which collapse to a narrow band just a few dB wide in this region for non-dimensional frequencies $\omega\nu/U_v^2$ greater than approximately 0.5 displaying, together, a clear -5 slope at the highest frequencies.

Values of U_v used to collapse the rough-wall pressure spectra are listed in table 4 and plotted in figure 15. The ratio of the shear friction velocity U_v to the conventional friction velocity U_τ exhibits consistent trends when plotted against roughness Reynolds number $k_g^+ = U_\tau k_g/\nu$, as shown in this figure. We see that for all the rough surfaces U_v/U_τ is less than one. For the present data, representing three rough surfaces with a sparseness $\lambda = 0.052$, this ratio decreases monotonically with increasing roughness Reynolds numbers starting at 0.75 for the 20 m s^{-1} flow over 1 mm hemispheres ($k_g^+ = 62$) and dropping to 0.58 for 60 m s^{-1} flows over the two 3 mm hemisphere surfaces ($k_g^+ \cong 500$). Together the variations for the three rough surfaces define a single curve. Also included in figure 15 and table 4 are values inferred from the measured spectra of other studies. These values are more scattered but, at the same time, represent a range of sparseness values. Values of U_v/U_τ for Varano's (2010) experiments ($\lambda = 0.013$, 0.025, 0.052 and 0.098) are rather scattered, but overall show a decrease as the roughness becomes more dense and the sparseness ratio is reduced. Although Blake (1970) did not give precise sparseness ratios for his surfaces, exactly the same trend is visible in the data obtained from his spectra, with the S-S (sparse-small) rough surface being associated with significantly larger values of U_v/U_τ than either of the dense roughness surfaces, D-S and D-L. Values of U_v/U_τ for Aupperle & Lambert's (1970) spectra stand apart from those of other experiments, being somewhat low and showing a gradually increasing trend with k_g^+.

Study	Surface	U_e (m s^{-1})	U_v/U_τ	Study	Surface	U_e (m s^{-1})	U_v/U_τ
	S-S	38	0.70		1 mm ordered	20	0.75
	S-S	50	0.68		1 mm ordered	30	0.72
Blake (1970)	D-S	38	0.60		1 mm ordered	40	0.70
Sand grains	D-S	50	0.58		1 mm ordered	50	0.68
	D-L	38	0.54		1 mm ordered	60	0.66
	D-L	50	0.52		3 mm ordered	20	0.67
					3 mm ordered	30	0.64
Aupperle	Grade 36	50	0.40	Present work,	3 mm ordered	40	0.62
& Lambert	Grade 12	50	0.48	hemispheres	3 mm ordered	50	0.60
(1970) Sand	Grade 4	50	0.50		3 mm ordered	60	0.58
grains					3 mm random	20	0.66
	Fetch 1	27	0.80		3 mm random	30	0.64
	Fetch 1	20	0.85		3 mm random	40	0.62
	Fetch 2	27	0.83		3 mm random	50	0.60
Varano (2010)	Fetch 2	20	0.93		3 mm random	60	0.58
Hemispheres	Fetch 3	27	0.80				
	Fetch 3	20	0.92				
	Fetch 4	27	0.93				
	Fetch 4	20	0.95				

TABLE 4. Values of U_v/U_τ determined by spectral fitting.

3.5. *Physical interpretation of the shear friction velocity*

A possible explanation of the above results is that viscous scales contributing to the pressure fluctuations at the wall, at locations not immediately adjacent to roughness elements, scale like those of a smooth-wall boundary layer $\omega\nu/U_\tau^2$ but with a friction velocity calculated without the contribution from the pressure drag on the roughness elements. This is consistent with the ratio U_v/U_τ being less than one for all rough surfaces, with it decreasing with roughness Reynolds number as the pressure drag on roughness elements increases, and with it increasing with the sparseness λ and thus the proportion of the wall that is smooth.

Starting with this interpretation it is possible to write down a relationship between U_v, U_τ, the sparseness ratio and the drag coefficient of the roughness elements. The overall wall shear stress τ_w can be broken down into the average drag force on each roughness element D, and the averaged substrate wall shear stress τ_v for which the element drag is excluded:

$$\tau_w = \tau_v + nD, \tag{3.2}$$

where n is the number of roughness elements per unit planform surface area. It can be noted that while the drag force D includes both pressure and viscous forces, the viscous contributions are expected to be relatively minor, while the averaged substrate wall shear stress τ_v is entirely composed of the viscous forces acting along the wall. Following Schlichting (1979), we assume that a particular roughness element can be usefully thought of as having a fixed drag coefficient $C_D = D/\bar{q}A$, where A is the frontal projected area of the roughness element and $\bar{q}$ is the dynamic pressure averaged over the height of the element. Recognizing that the sparseness ratio $\lambda = nA$ and the shear friction velocity $U_v = \sqrt{\tau_v/\rho}$ we obtain

$$U_\tau^2 = U_v^2 + \lambda C_D \bar{q}/\rho. \tag{3.3}$$

Note that in the case of the smooth wall equation (3.3) reduces to $U_\tau^2 = U_\nu^2$, since there are no roughness effects to account for.

To test the credibility of our physical interpretation, we have used (3.3) to estimate U_ν/U_τ for the hemispherical roughness cases of the present measurements. For this purpose we roughly approximate the value of $\bar{q}$ by using a one-seventh power-law profile $U/U_e = (y/\delta)^{1/7}$ to give

$$\bar{q} = \frac{1}{2}\rho U_e^2 \frac{1}{k_g}\int_0^{k_g}\left(\frac{y}{\delta}\right)^{2/7}\mathrm{d}y = \frac{7}{18}\rho U_e^2\left(\frac{k_g}{\delta}\right)^{2/7}. \tag{3.4}$$

This, of course, ignores the profile dependence on viscous and roughness scales. Since the boundary-layer thickness, edge velocity, friction velocity and roughness size are known, it is then only necessary to select the value of C_D to make a prediction. Generally speaking one would expect the drag coefficient to be a function of the roughness element shape, Reynolds number, and spacing, and thus a variable in (3.3). However, we are able to obtain reasonable estimates of the shear to friction velocity ratios for the present hemispherical roughness cases by choosing a constant drag coefficient of 0.26, see figure 15. This value is quite close to the drag measurement of Bennington (2004), implying $C_D = 0.3$, for an isolated 1.4 mm radius hemispherical roughness element at the bottom of a 39 mm thick boundary layer. This result appears to support to the physical picture proposed.

If we accept the above physical interpretation of U_ν, figure 15 shows that a remarkably large fraction of the wall drag is produced by viscous shear. Viscous effects appear responsible for approximately half of the drag ($U_\nu/U_\tau \cong \sqrt{2}$) at a roughness Reynolds number k_g^+ of approximately 100. At $k_g^+ = 500$ this fraction is approximately one-third and barely decreasing with Reynolds number. This finding appears consistent with Mehdi *et al.*'s (2010, 2013) assertion of the continuing importance of viscous effects in controlling the structure and scaling of the rough-wall boundary layer at high Reynolds numbers.

3.6. *The triple scaling hypothesis*

The new high-frequency viscous scaling of figure 14(*b,c*) appears to apply to all the published data sets for rough-wall boundary layers considered here. At the same time, the classical outer scaling appears to be the best choice to correlate the low-frequency part of the spectrum (figure 10*c,d*). Blake's (1970) scaling in its original form (figure 11*a,b*) or in the modified form of Varano (figure 12*a,b*) shows a somewhat less convincing collapse in the mid-frequency region, but the picture is clarified considerably if the data are restricted to the present results that combine the largest roughness Reynolds numbers and largest boundary-layer thickness to roughness size ratios.

The fact that there appear to be three scaling regions for a high-Reynolds -number fully rough turbulent boundary layer is not, in retrospect, so surprising. The low-frequency pressure fluctuations seem bound to be determined by the overall scales of the boundary layer. Similarly, the highest-frequency pressure fluctuations must be constrained ultimately by viscosity. What happens between these two limits will be determined by the roughness. If the roughness Reynolds number is large enough and the rough surface can be defined by a single length scale, then it seems inevitable that there will be an intermediate region where pressure fluctuations are primarily produced by turbulence shed from the roughness elements and will scale,

as Blake predicted, on the roughness element size and the effective flow velocity that the roughness elements experience. The fact that the pressure fluctuations in this region produce a spectrum with an almost linear $-4/3$ slope is, at this point, unexplained. It may be that this characteristic can be connected to the more general behaviour of a bluff body in a sheared turbulent stream.

The physical argument for three scaling regions requires that there be a large scale separation between the boundary-layer thickness, the roughness, and the viscous scales. Symbolically, $\delta \gg k_g \gg U_\nu/\nu$. What will happen then when the roughness has more than one scale? Consider, as a thought experiment, a surface composed of hemispherical roughness elements with dimples. It would seem that, as long as there is sufficient scale separation between the hemispheres and the dimples, and as long as the effective Reynolds number of the dimples remains large, then such a surface would have four scaling regions, with the two central regions being defined by the two sets of roughness scales. This may not be good news. One expects that many practical rough surfaces, particularly stochastic surface shapes, will be defined by a large range of poorly separated scales that even at very high Reynolds numbers may well overlap at the lower end with the scales of viscous dissipation. The results and arguments presented here suggest that such a boundary layer would have a fluctuating pressure field that at low frequencies scales on outer boundary-layer variables, but that at higher frequencies is unique to the rough surface producing it. Thus, such boundary layers may have no universal surface-pressure scaling, regardless of Reynolds number.

4. Conclusions

Experiments have been performed on series of high-Reynolds-number flat-plate turbulent boundary layers formed over rough and smooth walls. The rough walls consisted of sparse arrays of hemispherical bumps and included differences in size and distribution. The boundary layers were fully rough, yet the elements remained a small fraction ($<1.4\,\%$) of the boundary-layer thickness, implying conditions free of transitional effects. Detailed measurements were made of the wall-pressure fluctuations using an array of pinhole microphones. Analysis was performed, incorporating results from comparable boundary-layer studies, to reveal the form and scaling of the wall-pressure spectrum in the presence of roughness. The following conclusions are drawn.

(*a*) At low frequencies the wall-pressure spectrum of both rough- and smooth-wall boundary layers scales in the same way on the outer boundary-layer variables. Specifically we find that the spectrum of both types of boundary layers appears most similar in this region if plotted as $\phi(\omega)U_\tau/(\tau_w^2\delta)$ versus $\omega\delta/U_e$, at least for $20 \lesssim \omega\delta/U_\tau \lesssim 800$.

(*b*) At the highest frequencies the wall-pressure spectrum of both rough- and smooth-wall boundary layers has a universal viscous form $\phi(\omega)U_\nu^2/(\tau_\nu^2\nu)$ versus $\omega\nu/U_\nu^2$. This form is scaled by a single flow variable, termed the shear friction velocity U_ν where $\tau_\nu = \rho U_\nu^2$, and exists for $\omega\nu/U_\nu^2 \gtrsim 0.6$.

(*c*) In smooth-wall boundary layers U_ν is identical to the conventional friction velocity U_τ. In rough-wall boundary layers it is always less than U_τ and its ratio with it is a systematic function of the roughness Reynolds number and sparseness. Physically U_ν appears to be the friction velocity without the contribution from the pressure drag on the roughness elements, and estimates of its value based on this hypothesis realistically reproduce its observed variations. The dependence of U_ν/U_τ on roughness Reynolds number shows that the fraction

of the wall drag associated with viscous shear decreases only slowly with k_g^+ and is still approximately one-third at $k_g^+ = 500$. This appears consistent with Mehdi *et al.*'s (2010, 2013) assertion of the continuing importance of viscous effects in rough-wall boundary layers at high Reynolds numbers.

(*d*) At mid-frequencies the rough-wall boundary-layer pressure spectra are seen to have a third region in which Blake's (1970) scaling $\phi(\omega)U_\tau/(\tau_w^2 k_g)$ versus $\omega k_g/uU_\tau$ or the near relative proposed by Varano (2010) most closely correlates different rough-wall pressure spectra. The extent of this region grows with Reynolds number, but was seen to encompass at least $3 \lesssim (\omega k_g/U_\tau) \lesssim 20$ for the experimental cases considered here. Pressure spectra plotted on a log–log scale in this frequency range show the development of a $-4/3$ slope at higher roughness Reynolds number.

(*e*) The existence of three scaling regions in the rough-wall boundary-layer pressure spectrum appears inevitable if there is sufficient scale separation between the boundary-layer thickness, the roughness size, and the viscous scale. In cases where the roughness has two or more distinct and widely separated scales one might expect further scaling regions. Sufficiently complex rough surfaces may therefore result in complex pressure spectral forms that have no universal character in the mid- or high-frequency ranges even in the limit of high Reynolds number.

(*f*) The wall-pressure spectrum and boundary-layer parameters appear almost independent of roughness distribution, at least for the conditions covered in this study.

Acknowledgements

The authors would like to thank the National Science Foundation; in particular Dr H. Winter and Dr D. Papavassiliou, for their support under grants CBET-0853674 and CBET-1436088, as well as the Office of Naval Research, in particular Dr K.-H. Kim, for their support under grants N00014-08-1-0934 and N0014-13-1-0244.

REFERENCES

AUPPERLE, F. & LAMBERT, R. 1970 Effects of roughness on measured wall-pressure fluctuations beneath a turbulent boundary layer. *J. Acoust. Soc. Am.* **47**, 359–370.

BEARMAN, P. W. 1971 Corrections for the effect of ambient temperature drift on hot-wire measurements in incompressible flow. *DISA Information* **11**, 25–30.

BENNINGTON, J. L. 2004 Effects of various shaped roughness elements in two-dimensional high Reynolds number turbulent boundary layers. PhD dissertation, Aerospace and Ocean Engineering, Virginia Tech., http://scholar.lib.vt.edu/theses/available/etd-09032004-165611/.

BLAKE, W. 1970 Turbulent boundary layer wall-pressure fluctuations on smooth and rough walls. *J. Fluid Mech.* **44**, 637–660.

BLAKE, W. 1971 Turbulent velocity and pressure fields in boundary-layer flows over rough surfaces. In *Proceedings of the Symposium on Turbulence in Liquids*. 4–6 October 1971. University of Missouri-Rolla, edited by J. L. Zakin, 1971.

BLAKE, W. K. 1986 *Mechanics of Flow Induced Sound and Vibration*. Academic.

BRADSHAW, P. 1967 'Inactive' motion and pressure fluctuations in turbulent boundary layers. *J. Fluid Mech.* **30**, 241–258.

BULL, M. K. 1996 Wall pressure fluctuations beneath turbulent boundary layers: some reflections on forty years of research. *J. Sound Vib.* **190**, 299–315.

CHASE, D. M. 1980 Modeling the wavevector-frequency spectrum of turbulent boundary layer wall pressure. *J. Sound Vib.* **70**, 29–67.

CHOI, H. & MOIN, P. 1990 On the space-time characteristics of wall-pressure fluctuations. *Phys. Fluids* A **2** (8), 1450–1460.

CIPOLLA, K. M. & KEITH, W. L. 2000 Effects of pressure gradients on turbulent boundary layer wave number frequency spectra. *AIAA J.* **38** (10), 1832–1836.

CORCOS, G. M. 1963 Resolution of pressure in turbulence. *J. Acoust. Soc. Am.* **35** (2), 192–199.

CORCOS, G. M. 1967 The resolution of turbulent pressures at the wall of a boundary layer. *J. Sound Vib.* **6** (1), 59–70.

DEGRAAFF, D. B. & EATON, J. 2000 Reynolds-number scaling of the flat-plate turbulent boundary layer. *J. Fluid Mech.* **422**, 319–346.

DEVENPORT, W. J., BURDISSO, R. A., BORGOLTZ, A., RAVETTA, P. A., BARONE, M. F., BROWN, K. A. & MORTON, M. A. 2013 The Kevlar-walled anechoic wind tunnel. *J. Sound Vib.* **332** (17), 3971–3991.

DEVENPORT, W. J., GRISSOM, D. L., NATHAN ALEXANDER, W., SMITH, B. S. & GLEGG, S. A. L. 2011 Measurements of roughness noise. *J. Sound Vib.* **330** (17), 4250–4273.

DVORAK, F. A. 1969 Calculation of turbulent boundary layers on rough surfaces in pressure gradient. *AIAA J.* **7**, 1752–1759.

FARABEE, T. & CASARELLA, M. 1991 Spectral features of wall pressure fluctuations beneath turbulent boundary layers. *Phys. Fluids* A **3** (10), 2410–2420.

FARABEE, T. M. & GEIB, F. E. 1991 Measurements of boundary layer pressure fluctuations at low wavenumbers on smooth and rough walls. In *ASME Symposium on Flow Noise Modeling Measurement and Control, NCA*, vol. 11, pp. 55–68.

FERNHOLZ, H.-H. & FINLEY, P. J. 1996 The incompressible zero-pressure-gradient turbulent boundary layer: an assessment of the data. *Prog. Aerosp. Sci.* **32**, 245–311.

FLACK, K. A., SCHULTZ, M. P. & SHAPIRO, T. A. 2005 Experimental support for Townsend's Reynolds number similarity hypothesis on rough walls. *Phys. Fluids* **17**, 035102.

FOREST, J. 2012 The wall pressure spectrum of high Reynolds number rough-wall turbulent boundary layer. MS thesis, Aerospace and Ocean Engineering Department, Virginia Tech.

GEORGE, J. & SIMPSON, R. L. 2000 Some effects of sparsely distributed roughness elements on two-dimensional turbulent boundary layers. *AIAA Paper* 2000-0915.

GOODY, M. 2004 Empirical spectral model of surface pressure fluctuations. *AIAA J.* **42** (9), 1788–1794.

GRAVANTE, S. P., NAGUIB, A. M., WARK, C. E. & NAGIB, H. M. 1998 Characterization of the pressure fluctuations under a fully developed turbulent boundary layer. *AIAA J.* **36** (10), 1808–1816.

HERSH, A. S. 1983 Surface roughness generated flow noise. *AIAA Paper* 83-0786.

HUTCHINS, N., NICKELS, T. B., MARUSIC, I. & CHONG, M. S. 2009 Hot-wire spatial resolution issues in wall-bounded turbulence. *J. Fluid Mech.* **635**, 103–168.

JIMÉNEZ, J. 2004 Turbulent flows over rough walls. *Annu. Rev. Fluid Mech.* **36**, 173–196.

JIMÉNEZ, J. & HOYAS, S. 2008 Turbulent fluctuations above the buffer layer of wall-bounded flows. *J. Fluid Mech.* **611**, 215–236.

KILLEN, J. M. & ALMO, J. A. 1971 The influence of drag reducing polymer additives on surface pressure fluctuations on rough surfaces. *Project Rep.* 119. University of Minnesota, St Anthony Falls Hydraulic Laboratory.

KLEWICKI, J. 2013 Self-similar mean dynamics in turbulent wall flows. *J. Fluid Mech.* **718**, 596–621.

KLEWICKI, J., FIFE, P. & WEI, T. 2009 On the logarithmic mean profile. *J. Fluid Mech.* **638**, 73–93.

KLEWICKI, J. C., PRIYADARSHANA, P. J. A. & METZGER, M. M. 2008 Statistical structure of the fluctuating wall pressure and its in-plan gradients at high Reynolds number. *J. Fluid Mech.* **609**, 195–220.

LIGRANI, P. M. & BRADSHAW, P. 1987 Spatial resolution and measurement of turbulence in the viscous sublayer using subminiature hot-wire probes. *Exp. Fluids* **5**, 407–417.

MARUSIC, I., MONTY, J. P., HULTMARK, M. & SMITS, A. J. 2013 On the logarithmic region in wall turbulence. *J. Fluid Mech.* **716**, R3.

MCGRATH, B. E. & SIMPSON, R. L. 1987 Some features of surface pressure fluctuations in turbulent boundary layers with zero and favorable pressure gradients. NASA CR 4051.

MEHDI, F., KLEWICKI, J. C. & WHITE, C. M. 2010 Mean momentum balance analysis of rough-wall turbulent boundary layers. *Physica* D **239** (14), 1329–1337.

MEHDI, F., KLEWICKI, J. & WHITE, C. M. 2013 Mean force structure and its scaling in rough-wall turbulent boundary layers. *J. Fluid Mech.* **731**, 682–712.

MENEVEAU, C. & MARUSIC, I. 2013 Generalized logarithmic law for high-order moments in turbulent boundary layers. *J. Fluid Mech.* **719**, R1.

MEYERS, T. W. 2014 Wall pressure spectrum of high Reynolds number turbulent boundary layer flow over rough walls. MS thesis, Aerospace and Ocean Engineering Department, Virginia Tech.

MORTON, M. A. 2012 Rotor inflow noise caused by a boundary layer: inflow measurements and noise predictions. MS thesis, Aerospace and Ocean Engineering Department, Virginia Tech.

MULHEARN, P. J. 1976 Turbulent boundary layer wall-pressure fluctuations downstream from an abrupt change in surface roughness. *Phys. Fluids* **19**, 796–801.

NIKURADSE, J. 1950 Laws of flow in rough pipes. NACA Tech. Mem. 1292.

OWEIS, G. F., WINKEL, E. S., CUTBRITH, J. M., CECCIO, S. L., PERLIN, M. & DOWLING, D. R. 2010 The mean velocity profile of a smooth-flat-plate turbulent boundary layer at high Reynolds number. *J. Fluid Mech.* **665**, 357–381.

PANTON, R. & LINEBARGER, J. 1974 Wall pressure spectra calculations for equilibrium boundary layers. *J. Fluid Mech.* **65** (2), 261–287.

PANTON, R. L., GOLDMAN, A. L., LOWERY, R. L. & REISCHMAN, M. M. 1980 Low-frequency pressure fluctuations in axisymmetric turbulent boundary layers. *J. Fluid Mech.* **97**, 299–319.

RAUPACH, M. R., ANTONIA, R. A. & RAJAGOPALAN, S. 1991 Rough-wall turbulent boundary layers. *Appl. Mech. Rev.* **44** (1), 1–25.

SCHEWE, G. 1983 On the structure and resolution of wall-pressure fluctuations associated with turbulent boundary-layer flow Journal. *J. Fluid Mech.* **134**, 311–328.

SCHLICHTING, H 1979 *Boundary-Layer Theory*. McGraw-Hill.

SCHLOEMER, H. H. 1967 Effects of pressure gradients on turbulent-boundary-layer wall-pressure fluctuations. *J. Acoust. Soc. Am.* **42** (1), 93–113.

SCHULTZ, M. P. & FLACK, K. A. 2007 The rough-wall turbulent boundary layer from the hydraulically smooth to the fully rough regime. *J. Fluid Mech.* **580**, 381–405.

SIMPSON, R. L. 1973 A generalized correlation of roughness density effects on the turbulent boundary layer. *AIAA J.* **11**, 242–244.

SMITH, B. S. 2008 Wall jet boundary layer flows over smooth and rough surfaces. PhD dissertation, Aerospace and Ocean Engineering Department, Virginia Tech.

TSUJI, Y., FRANSSON, J. H. M., ALFREDSSON, P. H. & JOHANSSON, A. V. 2007 Pressure statistics and their scaling in high-Reynolds-number turbulent boundary layers. *J. Fluid Mech.* **585**, 1–40.

VARANO, N. D 2010 Fluid dynamics and surface pressure fluctuations of turbulent boundary layers over sparse roughness. PhD dissertation, Aerospace and Ocean Engineering Department, Virginia Tech.

WILLMARTH, W. W. 1975 Pressure fluctuations beneath turbulent boundary layers. *Annu. Rev. Fluid Mech.* **7**, 13–38.

WILLMARTH, W. W. & WOOLDRIDGE, C. E. 1962 Measurements of the fluctuating pressure at the wall beneath a thick turbulent boundary layer. *J. Fluid Mech.* **14**, 187–210.

WITTMER, K. S., DEVENPORT, W. J. & ZSOLDOS, J. S. 1998 A four sensor hot wire probe system for three component velocity measurements. *Exp. Fluids* **24**, 416–423; see also vol. 27, no. 4, pp. U1, September 1999.

YANG, Q. & WANG, M. 2013 Boundary-layer noise induced by arrays of roughness elements. *J. Fluid Mech.* **727**, 282–317.